RESEARCH ARTICLE

Fabrication and characterization of high molecular mass tmpe-based polyurethane wound dressing materials containing allantoin and gentamicin by electrospinning

Article history:
Received: 31-06-2023
Revised: 06-11-2023
Accepted: 14-12-2023

Ayşe Başak Çakmen[a], Samir Abbas Ali Noma[a], Canbolat Gürses[b], Süleyman Köytepe[a], Burhan Ateş[a], İsmet Yılmaz[c]

Abstract: In this study, biocompatible, antibacterial and high mechanical strength polyurethane-based wound dressing materials were prepared by using the electrospinning technique. In addition, allantoin and gentamicin which will contribute to wound healing, were incorporated into these fiber materials. Polyurethane structures containing trimethylolpropane ethoxylate (TMPE) with 2 different molecular weights were synthesized. TMPE-based polyurethanes/polycaprolactone (1:3) blends were also prepared by adding 1% gentamicin and 10% allantoin and they were knitted by the electrospinning method and turned into a wound dressing material. After this stage, chemical structure, morphological, thermal and mechanical properties, flexibility, antibacterial effect, *in vitro* biocompatibility, cell adhesion tests, allantoin release level, and biodegradability of the prepared wound dressing materials were performed. The prepared fiber materials exhibited antibacterial properties and 80% cell viability, approximately. In addition, the obtained wound dressing materials showed high mechanical strength and ideal gas permeability. For this reason, it offers an ideal alternative for closing wounds.

Keywords: Biomaterials; Wound dressing material; Biocompatibility; PU fibers; Electrospinning.

1. INTRODUCTION

Allantoin is a medically important compound with the formula $C_4H_6N_4O_3$. Symphytum species, also known as Comfrey, which are the main source of allantoin, are medicinal herbs belonging to the Boraginaceae family (Nastić *et al.*, 2020). Allantoin is known to be the active component of comfrey, which is responsible for triggering cell division and also promotes the growth of skin and subcutaneous tissue, bone and cartilage (Kimel *et al.*, 2023; Staiger, 2013). Allantoin contributes to wound healing by promoting cell division and the growth of connective tissues, bones and cartilage. In addition, allantoin is frequently used for cosmetic purposes due to its skin softening, balancing, repairing and healing effects (Kimel *et al.*, 2023; Staiger, 2013). Therefore, it is frequently used in cream form for biomedical purposes (Kimel *et al.*, 2023; Staiger, 2013). In all these applications, the main function of allantoin molecules is to support cell proliferation, promote extracellular matrix synthesis and reconstruct healthy

[a] Department of Chemistry, Science and Literature Faculty, Inonu University, Malatya, Turkey.
[b] Department of Molecular Biology and Genetics, Science and Literature Faculty, Inonu University, Malatya, Turkey.
[c] Department of Chemistry, Science and Literature Faculty, Inonu University, Malatya, Turkey.
Corresponding Author: ismet.yilmaz@inonu.edu.tr

tissue. Especially today, allantoin is widely used in the development of wound-covering creams, lotions as well as wound dressing materials.

Wound dressing materials are textiles that have the potential to be used in medical and surgical fields, designed in desired shapes and features to cover the wound area and meet certain needs (Singh *et al.*, 2013). The main aim of using wound dressing materials is to contribute to the healing of the wound by providing the most favorable conditions that will promote rapid wound healing and the most appropriate aesthetic repair possible (Yudanova & Reshetov, 2006). In addition, it should have a good antibacterial property to prevent possible infections and should have a structure that allows gas and liquid exchange (Liu *et al.*, 2017). Wound dressing materials are used for covering the wound surface by creating microbial control and a physical barrier to protect the wound from external influences, providing mechanical insulation by preserving the heat and moisture environment around the wound, absorbing excess wound fluid and the inherent odor of the wound, facilitating the healing of wounds and shortening the healing time (Deitzel *et al.*, 2001; Lionelli & Lawrence, 2003).

Wound dressings should be easily removable, should not stick to the wound, and should not cause trauma during changing stages (Nguyen *et al.*, 2023; Heyer *et al.*, 2013; Demarre *et al.*, 2015). They must be non-toxic, biocompatible, and biodegradable. Additionally, they should be non-allergenic, sterile, and suitable for continuous use. These dressings need to be easily accessible and affordable, aiming to reduce pain and meet the desired features effectively. An ideal wound dressing should mimic a smart device, displaying adaptability to treat various wounds. It should be capable of monitoring tissue conditions, actively contributing to the healing process, and even accelerating it. The dressing should ultimately restore the wound site to its former healthy structure and function (Mehteroğlu *et al.*, 2020; Dhivya *et al.*, 2015)

Depending on a wound type and its healing, the most appropriate wound dressing material system should be used (Boateng *et al.*, 2008). In general, different types of wound dressing materials can be used for rapid wound healing. Especially in recent years, nanofiber scaffolds are generally obtained from biocompatible as well as biodegradable natural and synthetic polymers or their mixtures (Mogaşanu & Grumezescu, 2014; Zahedi *et al.*, 2009). It is known that traditional wound dressing materials with many different features and types developed with technological developments are of great importance in wound healing and treatment. Besides, these dressing materials are sometimes insufficient to ensure effective wound healing and have a disadvantage because they cause trauma by damaging the newly formed tissue or tissues during dressing changes (Boateng *et al.*, 2008). In this regard, wound dressings prepared with new-generation design and production techniques have demonstrated their importance today. For this purpose, wound healing (wound closure and treatment) studies, which started with honey paste, herbal fibers and animal fats used for years to make wound dressings in the past, were replaced by traditional wound dressings in the following years. Today, new-generation wound dressing materials with more advanced performances are used (Chen & Chiang, 2010).

Modern (new generation) wound dressing materials have an understanding that has emerged in terms of contributing to the healing stages of the wound, accurately identifying the needs and requirements of the wound, providing the most appropriate response and the optimum moisture level (Bhoyar *et al.*, 2023). For this purpose, occlusive dressings such as alginate and hydrocolloids, foams, and hydrogels are widely used in the literature. Such wound dressing materials accelerate the formation of epithelial tissue, and the fact that this designed material has a structure similar to the body's own matrix forms the basis of studies on this subject (Lee *et al.*, 2014; Yao *et al.*, 2017; Kim *et al.*, 2016).

Various artificial and natural polymers have been designed as wound dressings that can provide wound healing in biomedical application areas (Pyun *et al.*, 2015; Miguel *et al.*, 2014; Chitrattha & Phaechamud, 2016; Chaturvedi *et al.*, 2016). In parallel with these developments, these materials still have different limitations such as poor mechanical properties, low absorption, poor anti-infective properties and many others, which can lead to infections, dehydration or maceration of wounds (Xu *et al.*, 2015). Among these, polyurethane-based wound dressing materials are widely applied in wound dressing due to their low cytotoxicity, good biocompatibility, high gas permeability, ideal mechanical properties and compatible flexibility (Xu *et al.*, 2016; Xu *et al.*, 2014; Sahraro *et al.*, 2016). When polyurethane and polycaprolactone are compared, they show good hydrophilicity and high mechanical properties due to stronger interactions resulting from their strong bond structures. In addition,

polyethylene glycol structures are frequently preferred today due to their excellent hydrophilicity and biocompatibility.

Electrospun nanomaterials play a crucial role in the field of biomedical applications. The effectiveness of electrospinning technology in biomedical contexts is undeniable, owing to key advantages such as high surface area to volume ratio, the production of continuous nanoscale fibers, a diverse range of applicable polymers, and the flexibility and versatility inherent in the electrospinning process. These advantages collectively contribute to the evolution of electrospinning in biomedical applications. One notable application lies in wound dressing, where electrospinning allows for the incorporation of bioactive agents or functional nanoparticles, expanding its utility (Yan *et al.*, 2011).

This study aims to produce wound dressing materials by electrospinning method using polyurethane, polycaprolactone and cross-linked PEGs, and also to develop a multifunctional biomaterial by adding allantoin, which has wound healing properties, and gentamicin sulfate, which is known to have antibacterial effects, to the wound dressing material. TMPE-450 structure was used to improve the flexibility, hydrophilicity, durability and drug-release properties of the polyurethane structure. In the first part of the study, two different molar masses of TMPE molecules namely Trimethylolpropane ethoxylate-450 (TMPE-450) and Trimethylolpropane ethoxylate-1014 (TMPE-1014) were used, and the effect of high TMPE molar mass on the material properties was examined. A non-aromatic, flexible and hyper-branched polyurethane structure was prepared by using Polyethylene glycol 200 (PEG), Tween 40 and Hexamethylene diisocyanate (HMDI) as monomers in addition to the TMPE molecule. Then, this polyurethane structure was mixed with polycaprolactone, allantoin and gentamicin and converted into a wound dressing material using the electrospinning technique. After the necessary structural and morphological characterizations of this obtained structure, wound healing efficiency and allantoin release kinetics were examined.

2. MATERIALS AND METHODS

2.1. Chemicals

Trimethylolpropane ethoxylate-450 (TMPE-450), Trimethylolpropane ethoxylate-1014 (TMPE-1014), Polyethylene glycol 200 (PEG), Tween 40, Hexamethylene diisocyanate (HMDI), Dimethylformamide (DMF), Tetrahydrofuran (THF), Dimethyl sulfoxide (DMSO), Triethylamine (TEA), Dichloromethane, Polycaprolactone (PCL), Gentamicin sulphate and Allantoin were obtained from Sigma-Aldrich chemical company.

2.2. Instrumentation

Fourier Transform Infrared Spectrophotometer (FTIR) was used for the structural characterization of the synthesized TMPE-based polyurethane structures and wound dressing materials. FTIR analyses were performed using Perkin Elmer. These FTIR analyses were performed using ATR mode in the spectral range of 400 - 4000 cm^{-1} with a sensitivity of 4 cm^{-1}. The surface and morphological properties of the obtained TMPE-based PUs and wound dressing materials were examined using a Scanning Electron Microscope (SEM) and Atomic Force Microscope (AFM). In SEM analyses, the surfaces of PU structures and wound dressing materials were coated with a Au/Pd spatter and measurements were made at different magnifications using LEVO-EVO SEM analyzer. Detailed surface analyses of PU and PU/PCL structures were elucidated by AFM analyses. Park System XE100 model AFM device was used in AFM analyses and the samples were analyzed in non-contact mode. Thermal properties of the obtained PU structures and PU/PCL wound dressing materials were analyzed with Shimadzu TGA-50 Thermogravimetric Analyzer, Shimadzu DTA-50 Differential Thermal Analysis and Shimadzu DSC-60 Differential Scanning Calorimetry devices. A heating rate of 10 °C/min was used in these analyses and all samples were analyzed in the platinum micro pan at static air atmosphere. In addition, the mechanical properties of these TMPE-based wound dressing materials were examined with the MTS E42 model Universal testing device. Mechanical analyses were performed in three replicates using samples with a cross-section of 120x10x0.1 mm, under room conditions and 60% humidity. Allantoin release levels were determined with the Shimadzu 1601 model UV Spectrophotometric device. Inovenso NS1 brand nanospinner device was used to electrospinning. During the determination of biocompatibility for the synthesized wound dressing materials, images of the cultured cells were taken using an Olympus CKX41 inverted microscope. Additionally, detailed structures of the synthesized hydrogels and their structure changes

during swelling were examined with a Triocular Soif Upright Metallogical microscope at up to 500X magnification. The cell culture studies were carried out with a Biotek Eon brand ELISA microplate reader. In addition, CO_2 incubator (Nüve), UV biosafety cabinet (Chemocell), and JuLI FL invert/fluorescent live cell analyzer were used in *in vitro* biocompatibility studies.

2.3. Polyurethane Synthesis

Polyurethanes with different tween ratios were prepared using, HDI, PEG 200 and TMPE structures in an inert atmosphere at 80 °C by reflux mechanism (Fig. 1 and Table 1). TMPE molecular mass was changed to 450 and 1014, and the effect of TMPE molar mass on the polyurethane structure and properties was examined. 3% allantoin and 1% gentamicin sulfate were added to the mixture prepared with a polyurethane/polycaprolactone ratio of 1:3. The obtained structures were characterized structurally, morphologically, and thermally. FTIR, SEM, AFM, TGA, DTA, and DSC techniques. The characterized polyurethane structures were transformed into a wound dressing material with an electrospinning method under optimum conditions (20 cm distance, 2 mL/h flow rate, and 20 kV operating voltage). It has been determined that wound dressing materials are biocompatible against L-929 cells in the cell culture experiment.

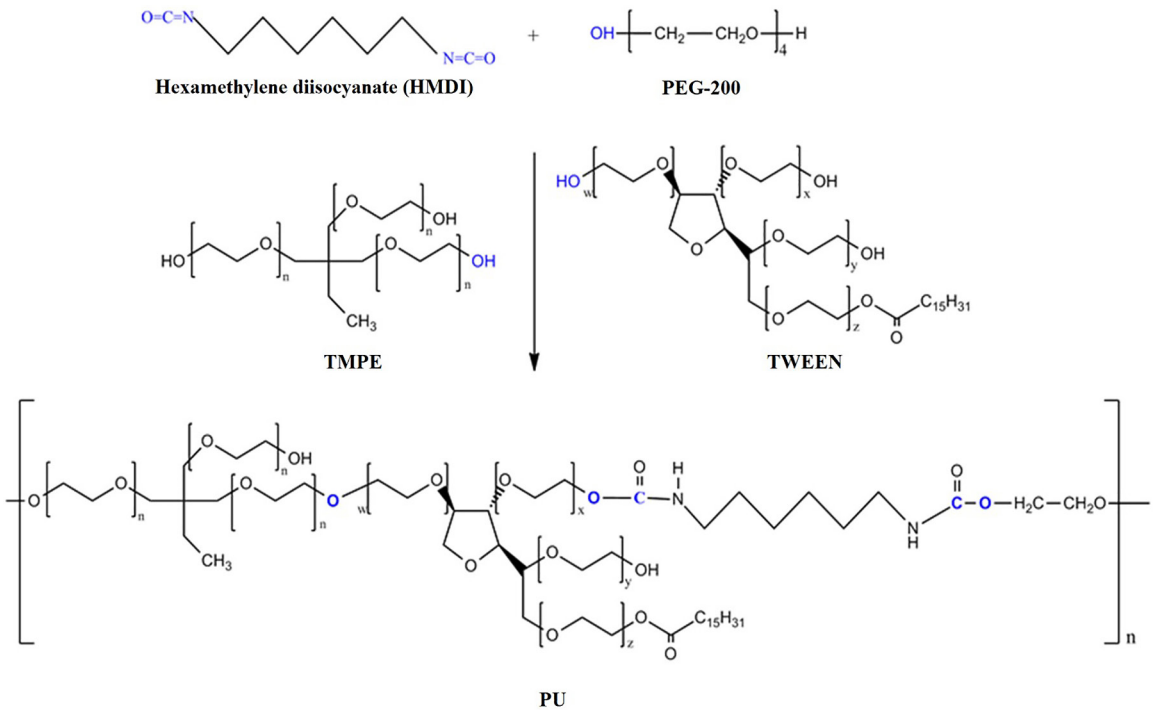

Figure 1. The synthesis and molar ratios of TMPE-based polyurethane structures.

Polymer	HMDI (%)	PEG 200 (%)	TMPE (%)	TWEEN 40 (%)
TMPE450-PU1	50	20	27.5	2.5
TMPE450-PU2	50	20	25	5
TMPE450-PU3	50	20	22.5	7.5
TMPE1014-PU1	50	20	27.5	2.5
TMPE1014-PU2	50	20	25	5
TMPE1014-PU3	50	20	22.5	7.5

Table 1. The molar ratios of TMPE-based polyurethane structures.

 https://doi.org/10.37819/nanofab.8.1787

2.4. Doping of Allantoin into Polyurethane/PCL

A total of 6 different PU structures were synthesized using two different TMPE ratios. Firstly, the prepared TMPE-based polyurethane (1 g) was dissolved in THF/DMF (50 mL, vol. ratio; 9/1) solvent mixture at room temperature and a homogeneous PU solution was obtained. Then PCL was added to this PU solution at a ratio of 1:3 (PCL:PU) and stirred for 3 hours. 10% of the total solid ratio of allantoin and 1% of gentamicin were added to the resulting mixture. The amounts of allantoin to be added to these polymer solutions were weighed at 10%, dissolved in 250 µL dimethyl sulfoxide (DMSO) solvent and added to the PU solution in solution form. A homogeneous solution was obtained by stirring for 1 hour at room temperature. This homogeneous solution was converted into wound dressing materials using the electrospinning technique. In the study, TMPE450-PU3-A:PCL and TMPE1014-PU2-A:PCL structures were prepared as wound dressing material in fiber formation by electrospinning technique using TMPE450-PU3 and TMPE1014-PU2 structures.

2.5. Doping of Gentamicin into Polyurethane/PCL

Gentamicin, which is the most widely used systemic antibiotic in the literature, was doped to the prepared polymer mixture to provide antibacterial properties (Pierchala *et al.*, 2018). The amount of gentamicin sulfate was adjusted to 1, 3 and 5 % Gentamicin and mixed at room temperature for 1 hour to distribute it homogeneously in the polymer solution. Then, this polymer solution was subjected to electrospinning to gain the samples' antibacterial properties.

2.6. Electrospinning of Polyurethane/PCL

Among the synthesized TMPE-based polyurethane structures, two structures as optimum structures were selected and transformed into wound dressing materials by electrospinning process. This process was carried out with an Inovenso brand laboratory type device designed according to the horizontal working principle in a cabin. First of all, the prepared TMPE-based polyurethane/PLC (molar ratio; 1/3) mixture was dissolved in THF/DMF (vol. ratio; 9/1) solvent mixture. The resulting solutions were transferred to 5 mL volume syringes. The polymeric solution was spun onto the collector plate with aluminum foil wrapped on it. The amount of solution fed into the electric field was determined as 2 mL/hour. The distance between the collector plate and the feeding unit was studied at different intervals of 15-20 cm and the optimum distance was determined as 15 cm. Electrospinning was tested at different electric field intensities of 18, 20 and 25 kV for each sample and fiber morphologies were checked. The experiments were carried out in the cabin at temperatures varying between 26-30 °C. This cabinet protects against unwanted external factors and helps prevent any electrical discharge.

2.7. Antibacterial Properties of Wound Dressing Materials

In this study, 6 different TMPE-based PU structures were synthesized. Based on structural, thermal and morphological investigations, TMPE450-PU3 and TMPE1014-PU2 structures were selected as the most ideal polyurethane structures. First of all, allantoin was added to these structures and wound dressing materials (TMPE450-PU3-A:PLC and TMPE1014-PU2-A:PLC) were created with PLC. Gentamicin was added to the obtained wound dressing materials to provide antibacterial activity. Effects of the synthesized TMPE450-PU3-A:PLC and TMPE1014-PU2-A:PLC structures on gram-negative (Escherichia coli) and gram-positive (Bacillus subtilis) bacteria were determined by measuring the zone diameters. In general, most of the research depending on antibacterial wound dressings have these two types of bacteria for the antibacterial activity assessments. In this context, the antibacterial properties of TMPE450-PU3-A:PCL and TMPE1014-PU2-A:PCL were determined by using fiber membrane disc. Each surface of the obtained discs was sterilized under UV light for 30 minutes and examined for antibacterial activity. For the antibacterial test, liquid bacterial cultures maintained with 0.5 McFarland turbidity standards were prepared by growing Escherichia coli (ATCC 25922) and Bacillus subtilis (ATCC 19659) bacterial species in Luria Bertani (LB) broth (10 mL) in a shaking incubator at 37 ºC for 24 hours. After the incubation process, one of the two bacterial species from 100 microliters of liquid cultures was transferred to a sterile nutrient (LB) agar medium separately in duplicate and spread with an L-shaped cell spreader under aseptic conditions. Polyurethane discs with/out gentamicin were placed on nutrient

(LB) agar petri dishes, where bacteria were cultivated, along with 1%, 3% and 5% of samples. According to the Disc Diffusion Method, Petri dishes were left in a static incubator at 37 ºC for 24 hours to observe the antibacterial effect. At the end of the incubation period, the effects of placed discs on bacteria were examined and the inhibition zone diameters were recorded using a millimetric ruler.

2.8. Allantoin Release Test of Wound Dressing Material

Allantoin release study was carried out with a Shimadzu 1601 model device. 1x1 cm of electrospun wound dressing materials were weighed and placed in 10 mL PBS buffer (pH: 7.4). The measurements were taken starting from the 1, 5, 10, 15, 30 minutes as well as 1, 2, 3, 4, 5, 12, 24, 48 to 72 hours. After every time interval, the PBS was recovered and replaced with an equal volume to maintain sink conditions during all studies.

2.9. Mechanical Strength Test of Wound Dressing Materials

The mechanical properties of TMPE450-PU3-A:PLC and TMPE1014-PU2-A:PLC electrospun fiber were measured using the MTS Systems E/CEED E42 model universal tensile testing device. Measurements were carried out at room temperature and a relative humidity of 60%. TMPE450-PU3-A:PLC and TMPE1014-PU2-A:PLC used in the measurements were cut to 20.0 mm in width, 50.0 mm in length and 0.5 mm in thickness. Mechanical test device parameters were used as 43.000 mm jaw distance, 0.847 mm/s tensile test speed, 10.0 Hz data collection rate, breaking force as MPa and breaking elongation value as mm. The test results were given with a stress-strain graph, with the module in kN/m^2 and the stress at break in mm/mm units. As a result of the mechanical tests, the values in elongation at break, breaking strength, and Young's modulus for wound dressing materials were calculated and interpreted according to the wound dressing type.

2.10. Biodegradability Properties of Wound Dressing Materials

In the biodegradability test, 0.1 g of samples were weighed, and films with a diameter of 1 cm were prepared and incubated in with 50 mM PBS buffer (pH: 7.4) at 37 °C. The biodegradability properties of the polymers were evaluated by calculating the percentage of lost mass at the end of the 1, 2, 3, 4 and 5 week incubation periods. Experimental measurements were done under ASTM (F1635-04) standards and the samples were studied in triplicate. Additionally, the biodegradation process was characterized by FTIR spectroscopy and SEM analysis techniques.

2.11. Biocompatibility Properties of Wound Dressing Materials in *In Vitro* Cell Culture System

In vitro biocompatibility tests were performed using indirect cytotoxicity assay in the cell culture system of wound dressing nanofibers prepared from synthesized polymers. *In vitro* cytotoxicity values of TMPE450-PU3-A:PLC and TMPE1014-PU2-A:PLC samples were determined by the indirect method using the spectrophotometer device using MTT [3-(4,5-dimethylthiazol-2-yl)-2,5-diphenyltetrazolium bromide] assay. The experimental protocol was prepared according to ISO-10993-5 "The Biological Evaluation of Medical Devices" standards. At this stage of the study, mouse (Mus musculus) fibroblast cells (L-929) were used. First, the TMPE450-PU3-A:PLC and TMPE1014-PU2-A:PLC samples were washed once in 70% ethanol and three times in sterile PBS (pH 7.4) buffer. Then, the samples were exposed to UV light for half an hour on each side. Later, the samples were incubated in DMEM (Dulbecco's Modified Eagle Medium) medium using an incubator containing 5% CO_2 at 37 °C for 72 h. L-929 cells, which reached the confluency of 80% 1 day before the end of the incubation period, were removed from the surface of the flasks with 0.25% trypsin-EDTA solution. After the cells were centrifuged at 2000 rpm for 5 minutes, 10^4 cells were seeded in each well of 96-well plates and incubated for 24 hours. At the end of the incubation period, DMEM medium of the cells was replaced with the medium in which the samples remained for 3 days, and an additional 24-hour incubation period was applied for the samples. After 1 day, the medium containing the cells was discarded and 90 µL of fresh DMEM was added to each well of the 96-well plates. Immediately afterward, 10 µL of MTT solution (5 mg/mL) prepared with sterile PBS was added to the wells and kept in an incubator containing 5% CO_2 at 37°C for 4 hours. Then, the medium containing MTT was removed from the

wells and 100 µL DMSO (dimethylsulfoxide) was added to each well to dissolve the formazan crystals formed as a result of the application of MTT substance, and the absorbance values at 540 nm were measured using a spectrophotometer device. DMEM medium, which was kept in the incubator for 72 hours apart from the samples, was added into the wells for the control group cells incubated under the same conditions as the samples, and the cells in these wells were considered 100% alive. As a result, the cell viabilities of the samples on L-929 cells were calculated compared to the control groups as follows:

% Viability = (optical density of the examined group / optical density of the control group) x 100

2.12. Cell Adhesion Assessments of Wound Dressing Materials

The cell adhesion assessments of polyurethane-based wound dressing materials were performed on L-929 cells for 7 days. Firstly, the wound dressing materials were sterilized with seventy percent of ethanol followed by UV for 1 hour. Then, the materials were placed onto 24-well plates. 500 µL of DMEM with 10% of FBS and 1% of Penicillin/Streptomycin mixture containing L-929 cells was poured onto the polyurethane-based wound dressing materials as 5×10^4 cells per well. Shortly after, the 24-well plates were incubated for 7 days at 37 ºC and 5% of CO_2. The media were replaced with fresh media every other day. One week later, the polyurethane based wound dressing materials were removed from the cells and washed with PBS. Then, SEM analysis was performed for the materials.

3. RESULTS

3.1. The Structural Analysis Results of TMPE450 and TMPE1014-based Polyurethanes

FTIR spectra of TMPE450-based polyurethane structures are given in Fig. 2(a). In these spectra, N-H stretching of the urethane bond was observed at 3000-3400 cm^{-1}. Peaks originating from aliphatic CH stretching vibration are clearly visible at 2850-2950 cm^{-1}. The urethane bond carbonyl stretching vibration is observed at 1780 cm^{-1}. At 1560 cm^{-1}, the stretching vibration is seen originating from the C=O bond related to NH groups. There is C-N-C stretching vibration at 1440 cm^{-1}. One very distinct C-O-C etheric stretching vibration is seen at 1250 cm^{-1}. Aliphatic CH stretching vibrations originating from the Tween structure are especially evident in 725 cm^{-1}. When all this peak distribution is evaluated in general, it is clearly understood that the desired polyurethane structure has been achieved. From the free isocyanate peak at 2260 cm^{-1} seen in the spectra in Fig. 2(a), it can be understood from the fact that the reactions are completed and there is no free isocyanate left in the final product. On the isocyanate spectra, each of the peaks originating from PEG, Tween and TMPE were seen. Fig. 2(a) confirms the desired structure.

IR spectra of polyurethane structures obtained using TMPE1014 monomer with a molecular mass of 1014 g/mol are given in Fig. 2(b). On this figure, it was first tested that the polymerization was completed and that there was no free monomer residue. In this context, the existence of free isocyanate peaks around 2220 cm^{-1} has been questioned. No free isocyanate peak was seen on all three spectra. It can be concluded from these three spectra that the polymerization is completed and there is no free isocyanate residue in the environment. The urethane group peaks of the formed polyurethane structure at 1775 cm^{-1}, urethane bond carbonyl stretching vibration at 1560 cm^{-1}, CO-NH stretching vibration at 1500 cm^{-1}, C-N-C stretching vibrations at 1440 cm^{-1} are seen. C-H stretching vibrations belonging to aliphatic groups in the polyurethane structure are seen as a double peak at 1845 and 1935 cm^{-1}. The CH stretching vibrations of aliphatic groups are also observed. The H bonds originating from the NH structure on the urethane groups in the range of 3000-3300 cm^{-1} can clearly be understood. All three polyurethane molecules obtained using TMPE1014 gave similar spectra because they contain similar bonds and structures. According to the obtained spectrum and peak values, it is clearly seen that the desired structure was synthesized.

Fig. 3(a) shows the TGA thermograms of TMPE450-PU structures. In these thermograms, it is seen that as the amount of tween on the TMPE structure increases, there are changes in the partial thermal stability of the TMPE450 based PU structure. Four different weight losses were observed in all three thermograms. The first weight loss has a value of approximately 3% that occurs between 50-200 °C. This weight loss is due to the removal of moisture trapped in the polymeric structure. The second weight loss observed between 230°C

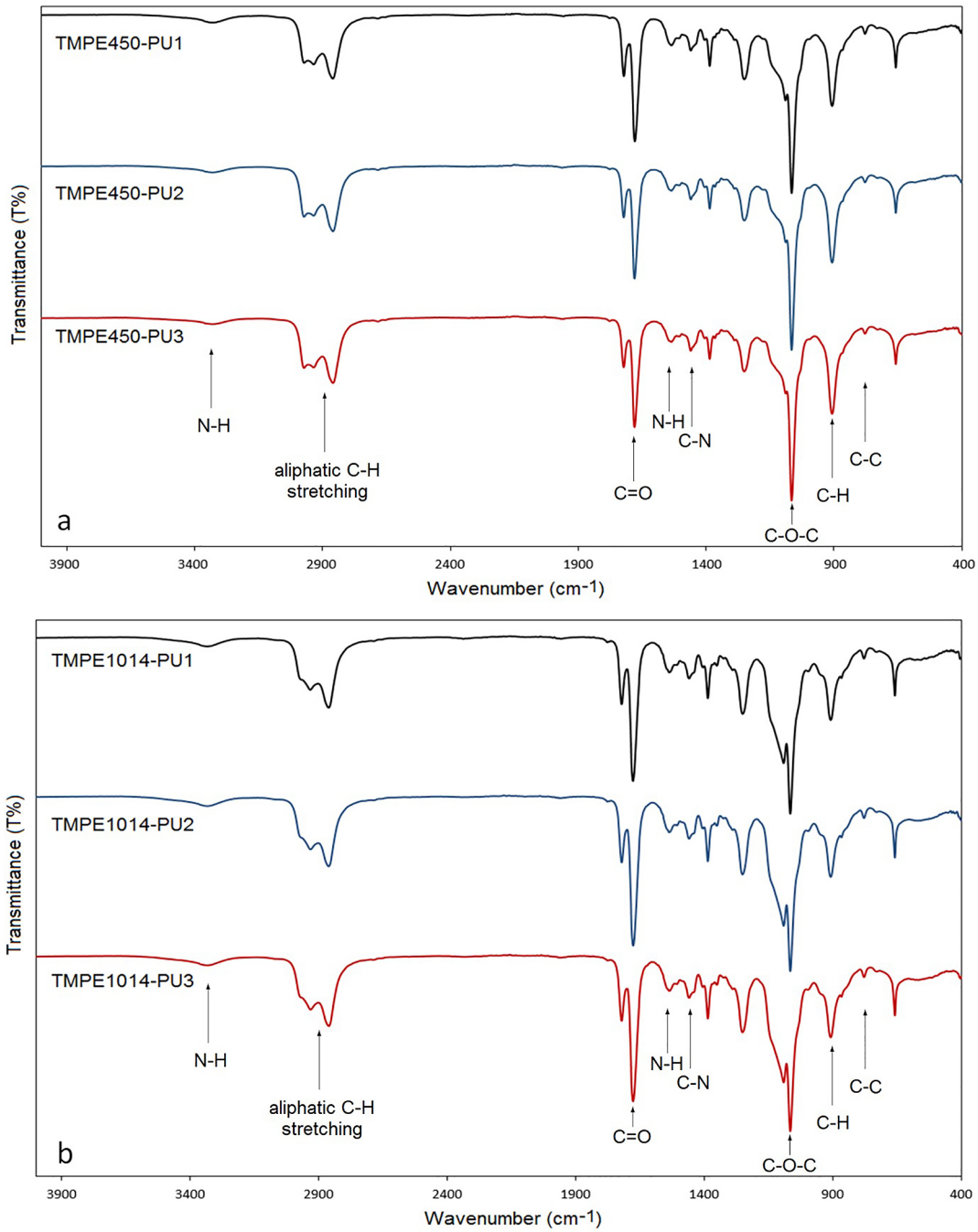

Figure 2. FTIR spectra of TMPE450 (a) and TMPE1014 (b) based PU structures.

and 355 °C is due to the degradation of hard segments in the polymer structure. The third and final weight loss occurs between 355°C and 485°C and is caused by thermal degradation of the soft segments in the polymer structure. The final weight loss is due to thermal degradation. The DTA thermograms given in Fig. 4(b) confirm these TGA thermograms (in Fig. 4(a)). Especially in DTA thermograms, four distinct exotherm peaks with four different weight loss intervals are observed. The first of these peaks arises from the degradation of the soft segments in the structure (Haryńska *et al.*, 2019). The second peak corresponds to the degradation of tween structures, and the third peak arises from the degradation of hard segments and thermal degradation of the polymeric structure.

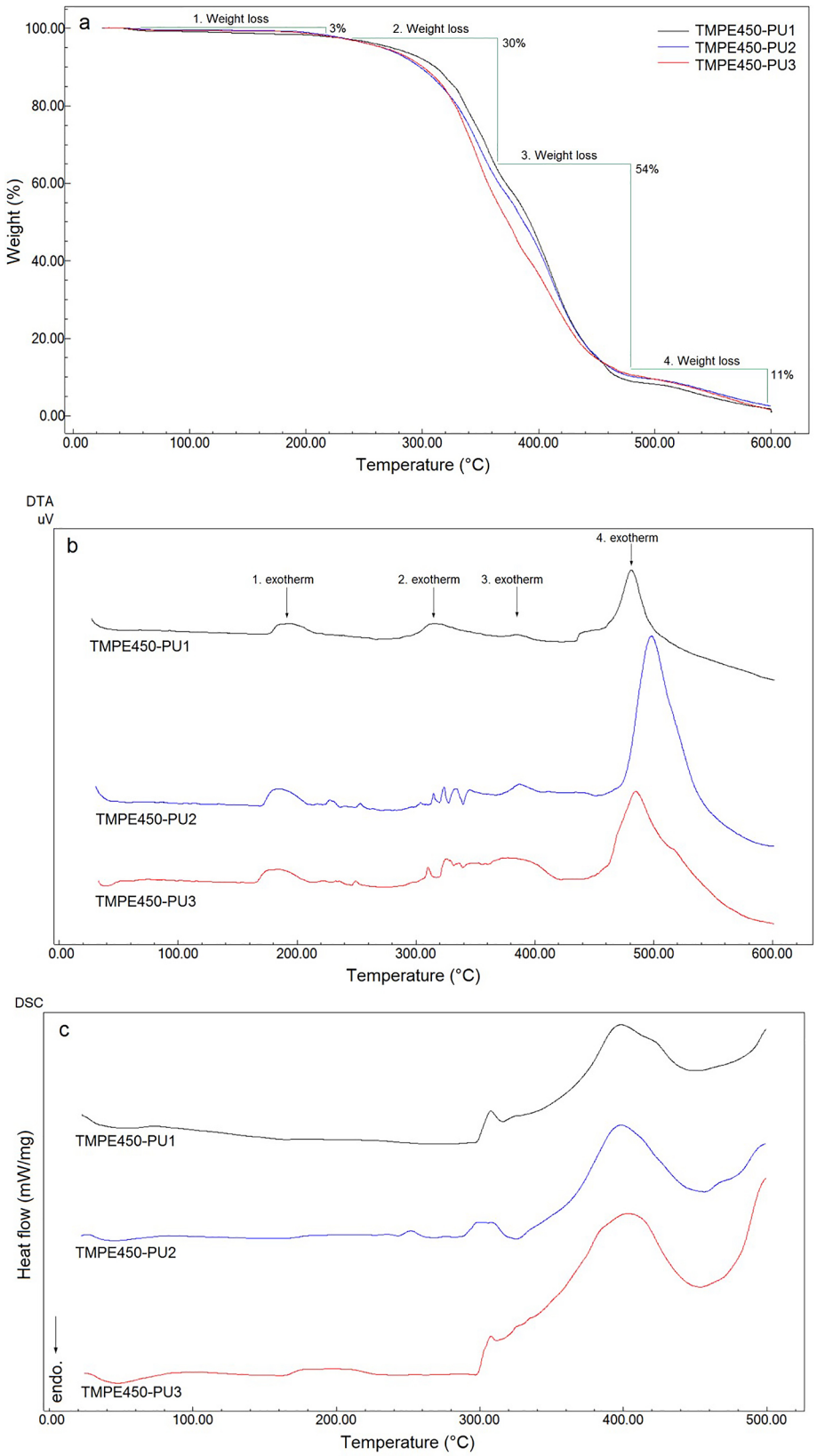

Figure 3. TGA (a), DTA (b) and DSC (c) thermograms of TMPE450 based PU structures.

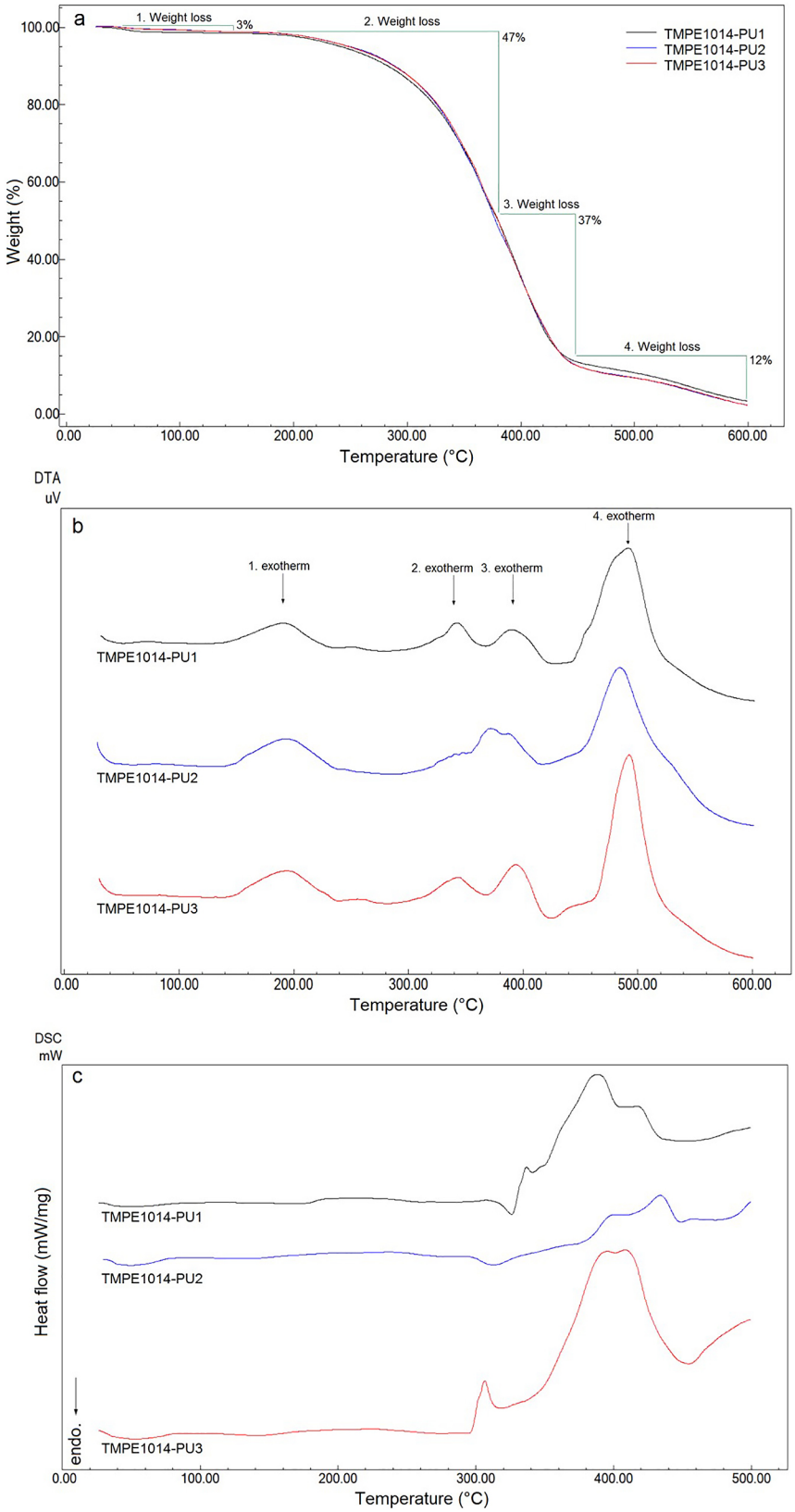

Figure 4. TGA (a), DTA (b) and DSC (c) thermograms of TMPE1014 based PU structures.

 https://doi.org/10.37819/nanofab.8.1787

DSC spectra of TMPE450-based PU structures are given in Fig. 4(c). These thermograms confirm the DTA thermograms. Additionally, when the DSC thermograms of TMPE450-based PU structures are examined, we see that the thermal stability of the obtained PU structures increases compared to monomeric structures (Fig. 4(c)). This increase in stability proves to us the formation of a high network structure. Similar verification can also be made from DTA thermograms. If a general interpretation is made according to thermal analysis, the general degradation temperature of the entire PU structure starts at approximately 200 °C. Therefore, intrinsic thermal stability appears to be around 200 °C. Accordingly, it is possible that the biomaterials to be obtained can be sterilized with steam.

The TGA thermograms of TMPE1014 based PUs are seen in Fig. 4(a). All three structures show four different weight losses. The first weight loss is around 100 °C and is due to the removal of moisture in the urethane structure. The second weight loss is a significant and sharp weight loss value that starts around 200 °C and continues until 360 °C. This is due to the degradation of the aliphatic-characterized polyurethane hydroxycarbon chains, which constitute the majority of the weight loss. The third weight loss is due to the degradation of the hard segments in the polyurethane structure and is generally seen in the range of 360-460 °C. Thermal degradation is completed between 460 and 600°C. The fact that all three structures give similar thermograms proves to us that the structures are shaped identically. Additionally, we understand from the thermograms in Fig. 4(b) that the thermal stability of the structure increases towards the TMPE1014-PU2 structure. Thermograms were obtained confirming the DTA data seen in Fig. 4(b). From these thermograms, the peaks are observed resulting from the degradation of soft segments, especially starting at 200 °C and ending at 450 °C, and then general polymeric degradation of hard segments around 450 and 600 °C. In Fig. 4(c), the DSC thermograms of TMPE-3-based polyurethanes are seen. Polymeric softening temperatures, which are very significant, especially for comparing the applicability of wound dressing materials, were determined with these measurements. An ideal wound dressing material should have durability close to body flexibility. With these studies, it was found that the Tg transitions of the polymer were below room temperature. This proves that polymers have appropriate flexibility.

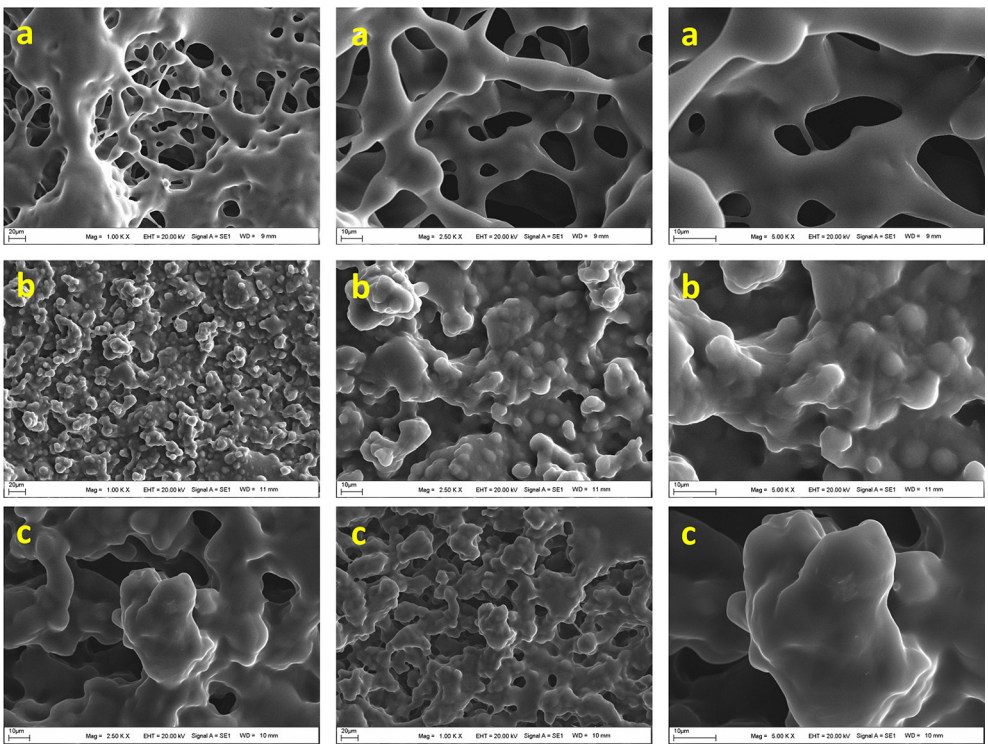

Figure 5. SEM images of TMPE450-PU1 (a), TMPE450-PU2 (b) and TMPE450-PU3 (c) structures with different magnifications (1000x, 2500x and 5000x).

Fig. 5a-c shows SEM images of TMPE450-based polyurethanes at different magnifications. In these images, it was determined that the structure was homogeneous, free of foreign objects, and had suitable film morphology. In these images, a pure and uniform polyurethane structure is seen. The structures exhibit a globular structure in certain regions and a porous, extremely branched structure in certain regions. These images show that the polyurethane structure is suitable for the tissue scaffold morphology. A generally porous structure prevails in all TMPE-based PU, which is diversified according to tween ratios. In addition, the surface is homogeneous and rough. When magnification is made in more detail, the surface cavities become quite clear. At high magnifications, TMPE450-PU1 structures appear to resemble natural hydrogel structures. In addition, the porosity that periodically appears in the TMPE450-PU2 structure positively affects the biocompatibility feature of polyurethane.

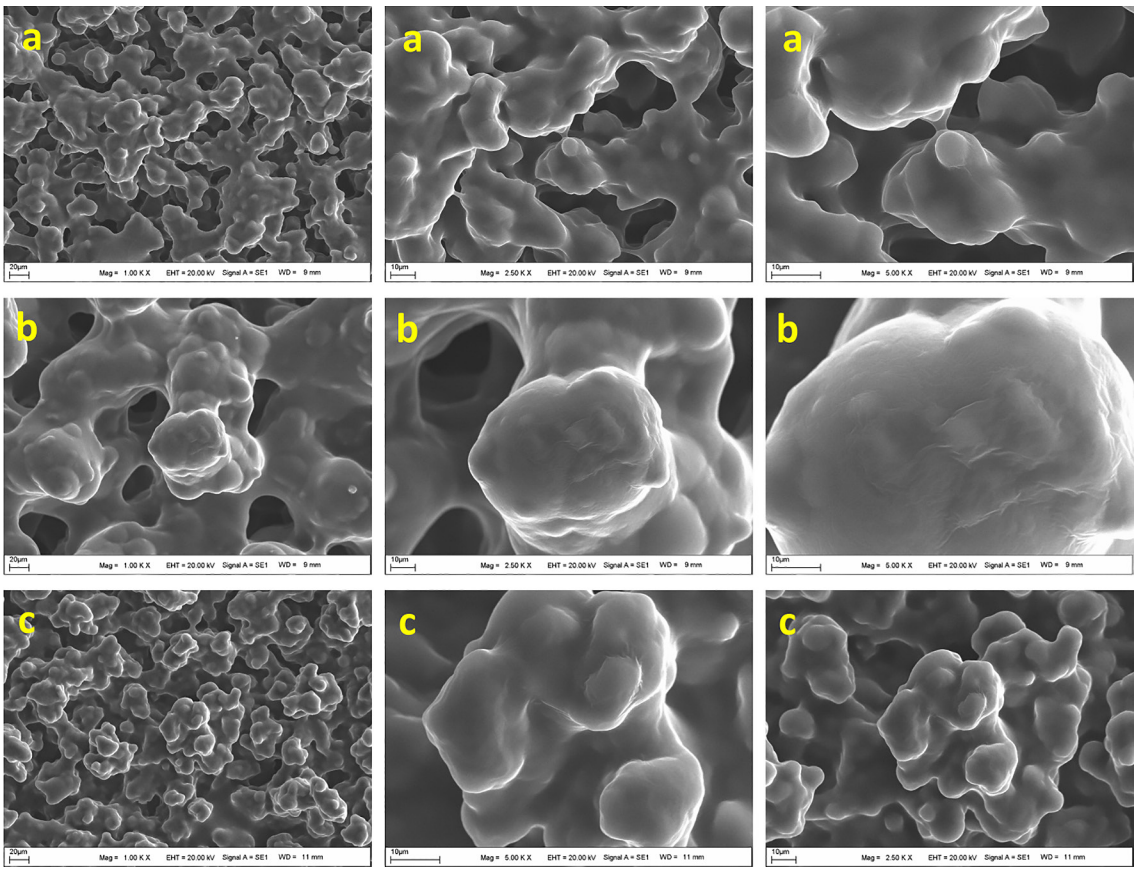

Figure 6. SEM images of TMPE1014-PU1 (a), TMPE1014-PU2 (b) and TMPE1014-PU3 (c) structures with different magnifications (1000x, 2500x and 5000x).

Fig. 6a-c shows SEM images of TMPE1014 structured polyurethanes at different magnifications. In these images, it was determined that the structure was homogeneous, free of foreign objects, and had a rough morphology. All three polymers contain dense porosity and globular cavities in their structure. In particular, the TMPE1014-PU3 structure has a densely porous and rough structure, containing a higher surface area. Therefore, the TMPE1014-PU3 structure shows an ideal drug release system structure. When all these findings were evaluated in general, the TMPE450-PU3 structure was preferred in terms of its film property, thermal stability and softening temperature. In the relevant group, this polymer structure was used for electrospinning

TMPE450-PU3 from the TMPE450 group and TMPE1014-PU2 structure from the TMPE1014 group were preferred as wound dressing materials for further studies. Firstly, the relevant polyurethane structures were mixed with the polycaprolactone structure and subjected to the spinning

process. Then, prepared wound dressing materials were structurally characterized. While FTIR spectra were used for chemical characterization processes, TGA, DTA, DSC thermograms were taken for thermal characterization processes. SEM and AFM techniques were used to elucidate the surface and morphological structures of wound dressing materials. In addition, the mechanical properties of all three structures were determined by tensile stress testing with the Universal mechanical test device. Moreover, the biocompatibility, biodegradability, and antibacterial properties of the structurally characterized wound dressing materials were also revealed. All analysis results obtained are given below.

3.2. The Structural Characterization of Electrospun PU/PCL Wound Dressing Materials

In Fig. 7, FTIR spectra of PU/PCL fiber structures are given comparatively. In these spectra, peaks belonging to the PU and PCL groups in the fiber structure are seen. Besides, since the fiber structure obtained is considered as a wound dressing material, it should not contain monomer residues and free isocyanate groups. When the given FTIR spectrum is examined, the isocyanate peak observed at 2260 cm^{-1} in the monomeric isocyanate structure is not seen in the polymer structure. For this reason, there are no free monomer and isocyanate groups left in all three PU/PCL fiber structures. When evaluated structurally, the C-H peak originating from linear alkyl groups in polymeric fiber structures is observed at 2800-2900 cm^{-1} (Haryńska *et al.*, 2019). Carbonyl stretching vibrations originating from the urethane bond are clearly seen at 1720 cm^{-1}, and C-N-O vibrations originating from the urethane bond are seen at 1510 cm^{-1}. C-N stretching vibrations in all three structures are observed at 1440 cm^{-1}. These three stretching vibrations prove to us that urethane groups are included in the fiber structure (Haryńska *et al.*, 2019). Another proof that polyurethane groups are included in the fiber structures is that the C-O-C vibrations at 1270 cm^{-1} appear to originate from the PEG structure. Because of the polymeric structure, the hydroxyl characterization has changed and this change is due to hydrogen bonds. Especially, the appearance and intensity of broad bands resulting from the hydrogen bonds of N-H and –OH groups in the range of 3000-3300 and 3300-3600 cm^{-1} in the pure polyurethane structure changed with the PCL structure. This change is an important finding showing that PCL groups are included in the structure (Haryńska *et al.*, 2019). Another important finding is that the C=O stretching peak originating from the PCL structure is included in the spectrum structure at 1820 cm^{-1}.

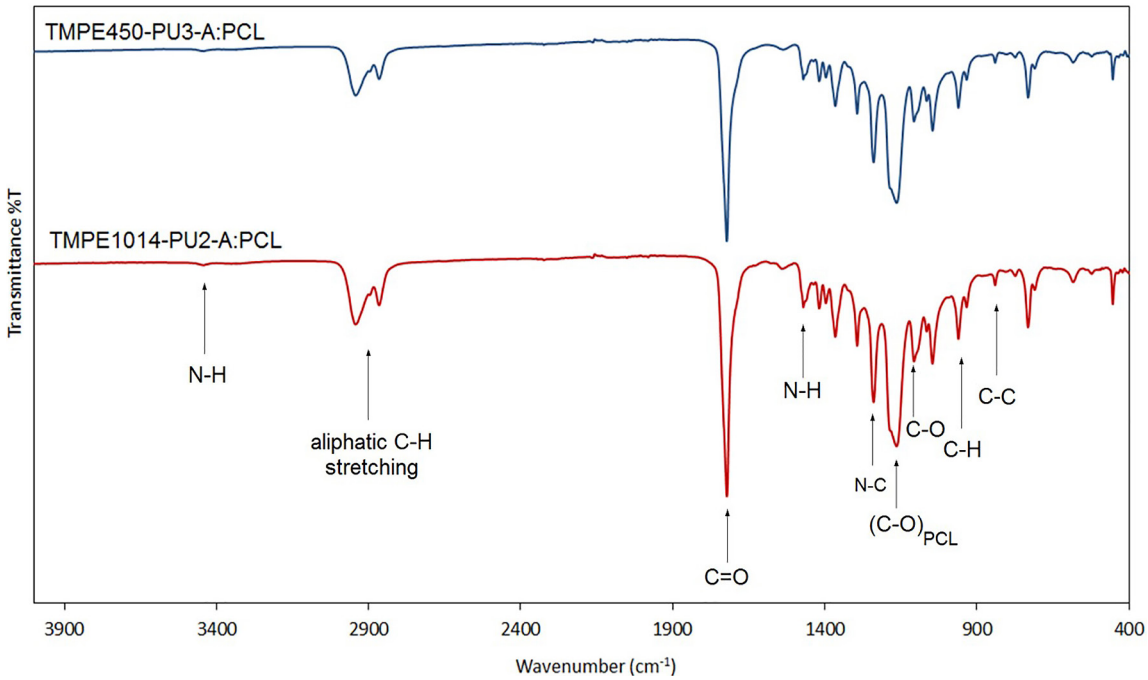

Figure 7. FTIR spectra of PU/PCL wound dressing materials.

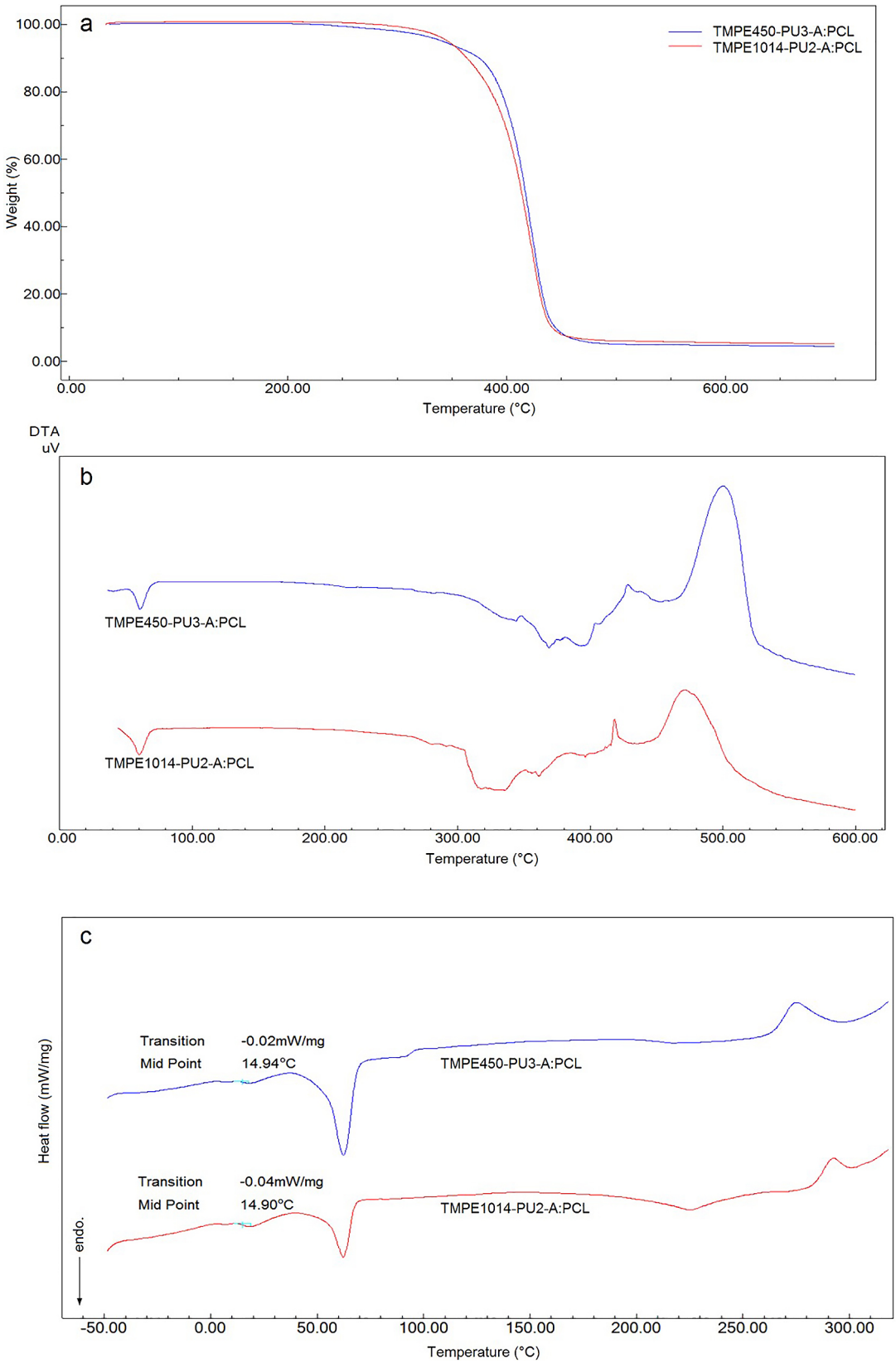

Figure 8. TGA (a), DTA (b) and DSC (c) spectra of PU/PCL wound dressing materials.

 https://doi.org/10.37819/nanofab.8.1787

Thermal properties of the materials to be electrospun are important in terms of parameters such as thermal stability, product sterilization, shelf life and flexibility of the wound dressing material. For this reason, the thermal properties of the polymeric fiber structured wound dressing materials obtained within the scope of the research were determined by TGA, DTA and DSC thermograms, respectively. The results of these analyses are given in Fig. 8(a), Fig. 8(b) and Fig. 8(c). The thermal stability of the synthesized PU/PCL wound dressing materials was determined by TGA analysis. According to the TGA thermogram given in Fig. 8(a), four main weight losses are observed in the case of the polymeric fiber structure. The initial weight loss is between 50 and 120 °C, and this is due to the removal of moisture present in the fiber structure. The second weight loss is observed between 210-270 °C and is caused by the degradation of soft segments. The third weight loss which occurs between 360-400 °C results from the thermal degradation of the PCL groups in the structure. The final weight loss is due to the degradation of hard segments approximately at 400-500 °C. Compared to the synthesized PU/PCL polyurethane structures, three basic weight losses are observed in the TGA thermograms of pure polyurethanes. The one more weight loss seen in the thermogram is due to the PCL groups in the fiber structure. This weight loss is compatible with the thermograms of pure PCL structures found in the literature; therefore it proves the presence of PCL groups in the structure. Depending on the weight loss value of PCL, it is understood that approximately 20% of PCL is included in the fiber structure. Another significant finding obtained from the relevant thermograms is the thermal stability of wound dressing materials. According to these thermograms, TMPE-structured PU/PCL fiber structures are thermally stable up to approximately 202 °C. This result shows that the obtained wound dressing materials are suitable for steam sterilization.

Fig. 8(b) shows DTA thermograms of TMPE-based PU/PCL wound dressing materials. These thermograms are seen to be compatible with the TGA thermograms given in Fig. 8(a). Three different exotherms are seen on these DTA thermograms. In addition to these exotherms, there is an endotherm observed between 50°C and 90°C, depending on the PCL groups present in the structure. Since this peak is not seen in the TGA thermogram, it is a phase transition and arises from the phase transition of PCL groups. The first exotherms seen in the DTA thermogram are observed between approximately 208-270°C and are caused by the decomposition of soft segments. The second exotherm occurs between 370-400°C and is caused by the degradation of the PCL structure. The last exotherm is between 400-500°C and is caused by the degradation of hard segments and thermal decomposition of the polymeric structure.

To determine the softening, melting temperatures and Tg values of the fiber structures obtained by electrospinning, DSC analyses were carried out under a static air atmosphere at a heating rate of 5 °C/min. These DSC thermograms are given comparatively in Fig. 8(c). When the DSC thermogram was examined, Tg transition value of the pure polyurethane structure was determined as 18.53 and 35.16 ° C for two different polyurethanes, respectively. Besides, in the DSC thermogram of polyurethane/PCL fiber structures, two different Tg transition values were observed at 14.81 °C and 25.95 °C, respectively. The first Tg value belongs to the PU structure and the second Tg value originates from the PCL structure. This result proves that a double polymeric structure was obtained.

The surface properties and morphological structure of TMPE-structured PU/PCL fibers were characterized by SEM analysis and the SEM images are shown in Fig. 9 and Fig. 10. Fiber SEM images of the TMPE450-PU3-A:PCL structure are given in Fig. 9. The fibers are homogeneous, widespread and uniformly sized at both low and high magnifications. The fiber structure is sharp and varies between approximately 1100 nm and 2050 nm. Small droplets and intersection points were seen on the fibers in some places. However, the fiber structure is smooth and homogeneous and does not contain any foreign objects. The entire structure has a fiber appearance.

Fig. 10 shows the SEM images of the fiber structures of TMPE1014-PU3-A:PCL. The fibers on this structure are quite common, smooth and sharply lined. It can be seen that the resulting fibers are much thinner, ordered and smoother with an average fiber diameter of 1050 ± 400 nm. Fiber size distribution was seen to be more uniform and finer than other structures. Optical images of all obtained fiber structures were recorded at different magnifications with an upright optical microscope. Especially at high magnifications, the smooth and homogeneous structure of fibers is seen.

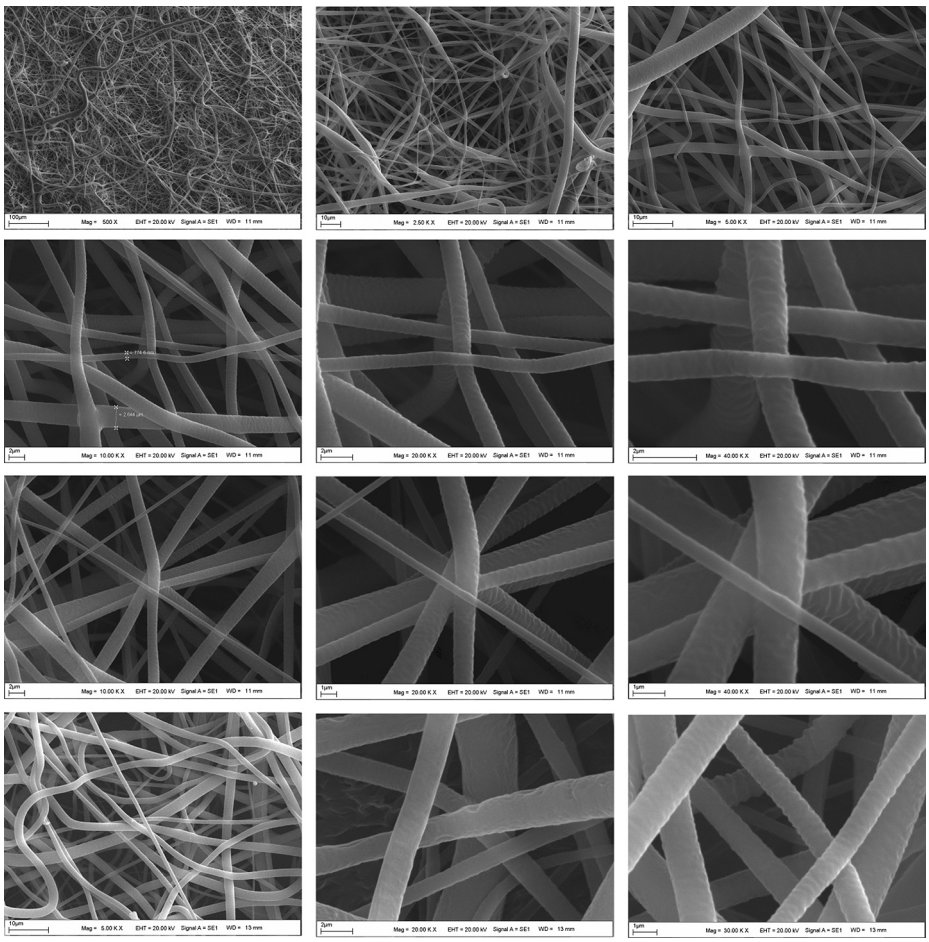

Figure 9. SEM images of the prepared TMPE450-PU3-A:PCL structures under a constant distance of 15 cm between the tip and the collector plate in the different magnifications.

Data regarding fiber diameters taken from SEM images are graphed, and the fiber size distributions for TMPE450-PU3-A:PCL and TMPE1014-PU3-A:PCL structures are shown in Fig. 11(a) and Fig.11(c). As a result of SEM images, the average polymer fiber diameters were found to be 1328 ± 349 and 1495 ± 492 nm for TMPE450-PU3-A:PCL and TMPE1014-PU3-A:PCL. It is seen that the morphology, physical and chemical properties of fibers change depending on different ratios. It has been determined that the diameters of the fibers obtained vary in direct proportion to the molecular weight of TMPE in the structure. Additionally, the fiber structures were confirmed by AFM measurements and are given in Fig. 11(c) and Fig. 12(d). According to AFM measurement, the mean diameters for the electrospun fibers were as follows 1.34 ± 0.39 μm and 1.43 ± 0.50 μm for TMPE450-PU3-A:PCL and TMPE1014-PU3-A:PCL, respectively. Moreover, when Fig. 11c and Fig.12d were examined, it was seen that the surface roughness in the AFM images of TMPE1014-PU3-A:PCL increased significantly compared to the TMPE450-PU3-A:PCL structure.

3.3. The Mechanical Properties of Electrospun PU/PCL Wound Dressing Materials

PU/PCL fiber structures should show sufficient flexibility and softening properties to be used for such a purpose. This point is especially necessary for wound and patient comfort. The dressing material applied to the wound should show stretching and tensiling behavior along with physical body movements. For this reason, mechanical tensile tests of the prepared wound dressing materials were carried out at room temperature in a static air atmosphere, and the results were given comparatively in Fig. 12. The constant strain rates during tensile tests were performed to determine the mechanical

 https://doi.org/10.37819/nanofab.8.1787

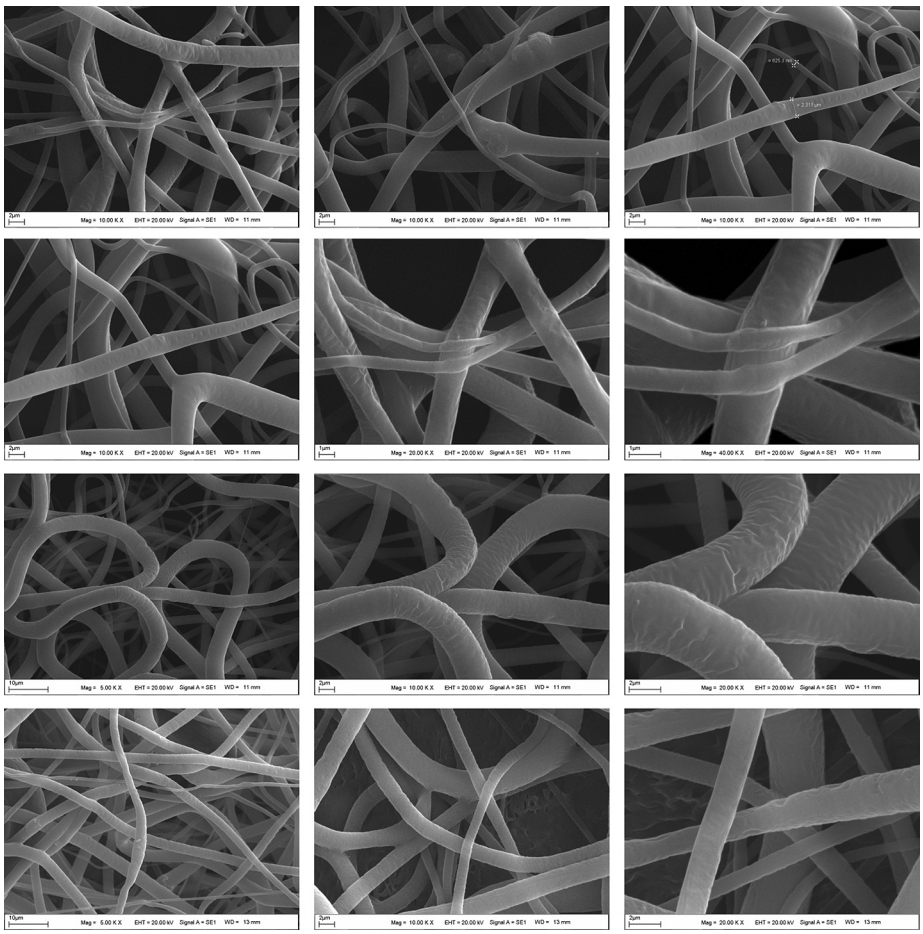

Figure 10. SEM images of TMPE1014-PU3-A:PCL structures under a constant distance of 15 cm between the tip and the collector plate in the different magnifications.

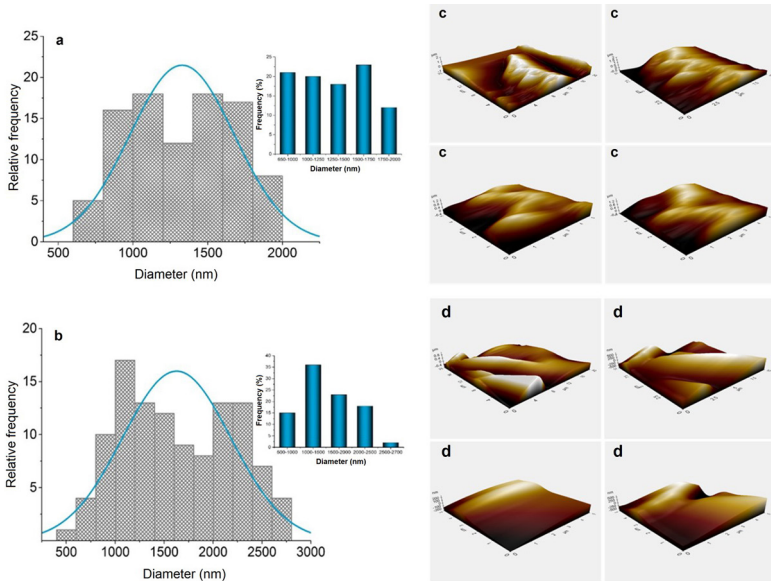

Figure 11. Fiber size distribution of TMPE450-PU3-A:PCL (a) and TMPE1014-PU3-A:PCL (b) structures. AFM images of TMPE450-PU3-A:PCL (c) and TMPE1014-PU3-A:PCL (d) structures.

properties of electrospun fiber structural materials, especially rupture, tensile strength and extension of Young's modulus. When these results were compared with the mechanical test results of pure PCL structured fibers in the literature, it was found that the addition of TMPE-structured PU groups affected the mechanical properties as can be seen from the stress-strain curves (Fig.12(a)). According to Fig. 12(b), for TMPE450-PU3-A:PCL and TMPE1014-PU2-A:PCL samples it was 3.67 ± 0.75% and 4.04 ± 0.90%, respectively. The tensile strength and Young's modulus of M images of TMPE450-PU3-A:PCL (c) and TMP structures were found to be (1.35 ± 0.14 and 0.44 ± 0.02 MPa)

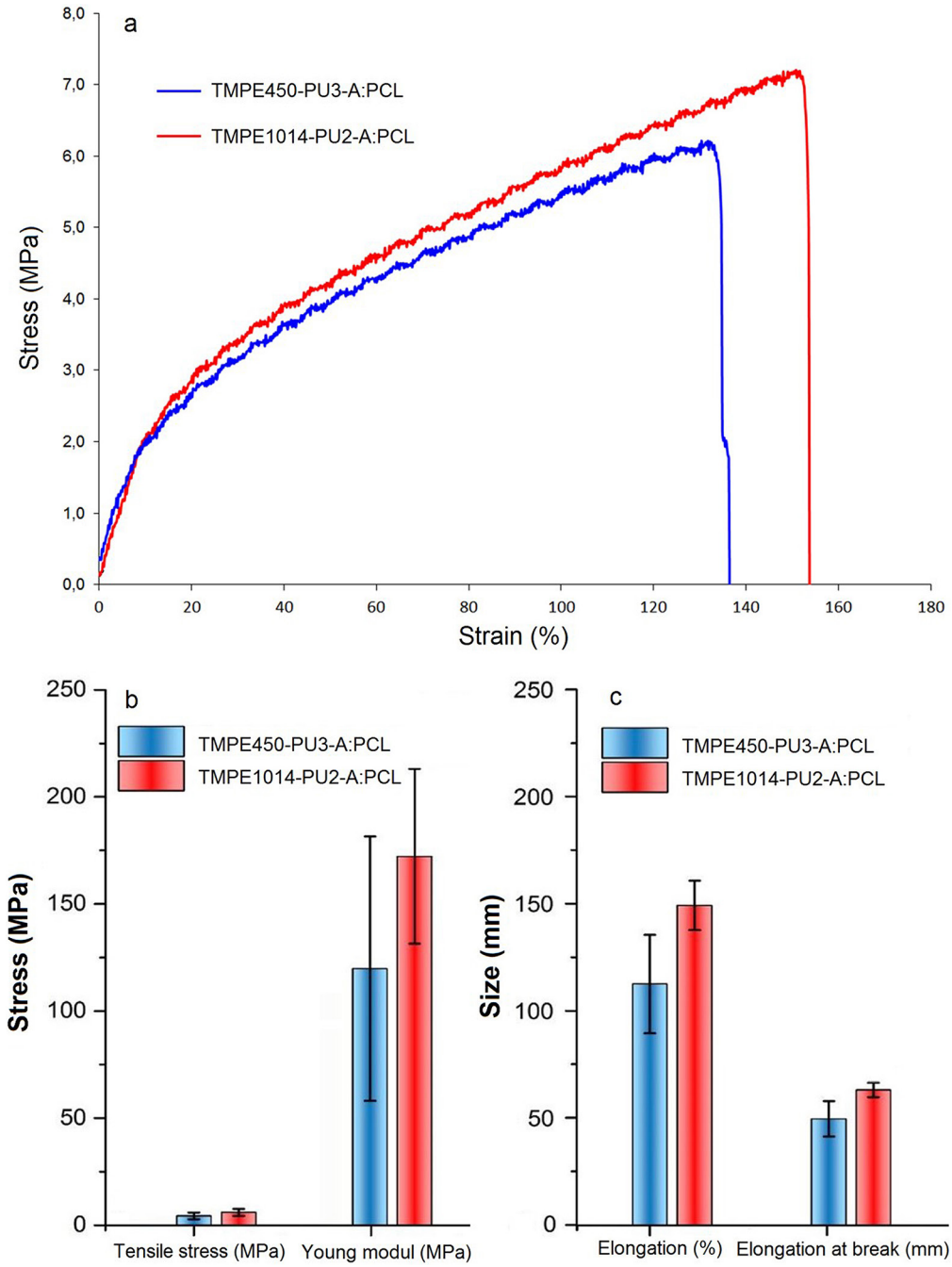

Figure 12. Breaking force, Young's modulus, elongation (%) and elongation at break graphs of TMPE450-PU3-A:PCL and TMPE1014-PU2-A:PCL samples.

 https://doi.org/10.37819/nanofab.8.1787

and (1.42 ± 0.12 and 0.53 ± 0.06 MPa), respectively. With the addition of the TMPE structure, the elongation, breaking stress and Young's modulus values of the pure PCL structure fibers increased. The most important reasons for this increase were the inclusion of PU groups, which were flexible and had higher mechanical strength than the PCL structure, and the presence of TMPE groups that created excessive branching points. When an intra-group evaluation was made, it was seen that M images of TMPE1014-PU3-A:PCL structure had higher elongation, breaking strength and Young's modulus than TMPE450-PU3-A:PCL structure. The reason for this is that it provides higher molecular mass and interchain interactions during polymerization.

3.4. Allantoin Release Properties of Electrospun PU/PCL Wound Dressing Materials

Fig. 13 shows the allantoin release results of wound dressing materials. The wound dressing material releases approximately 20% of the total loaded allantoin in approximately 50 hours. This rate can continue to be released regularly up to approximately 90%. In addition, the release graph reached the regular release value after 10 hours. These results are suitable for the desired allantoin level during application and the need for regular medication Afterward, another important finding is that the material obtained has the potential to be used in cases requiring long-term allantoin release.

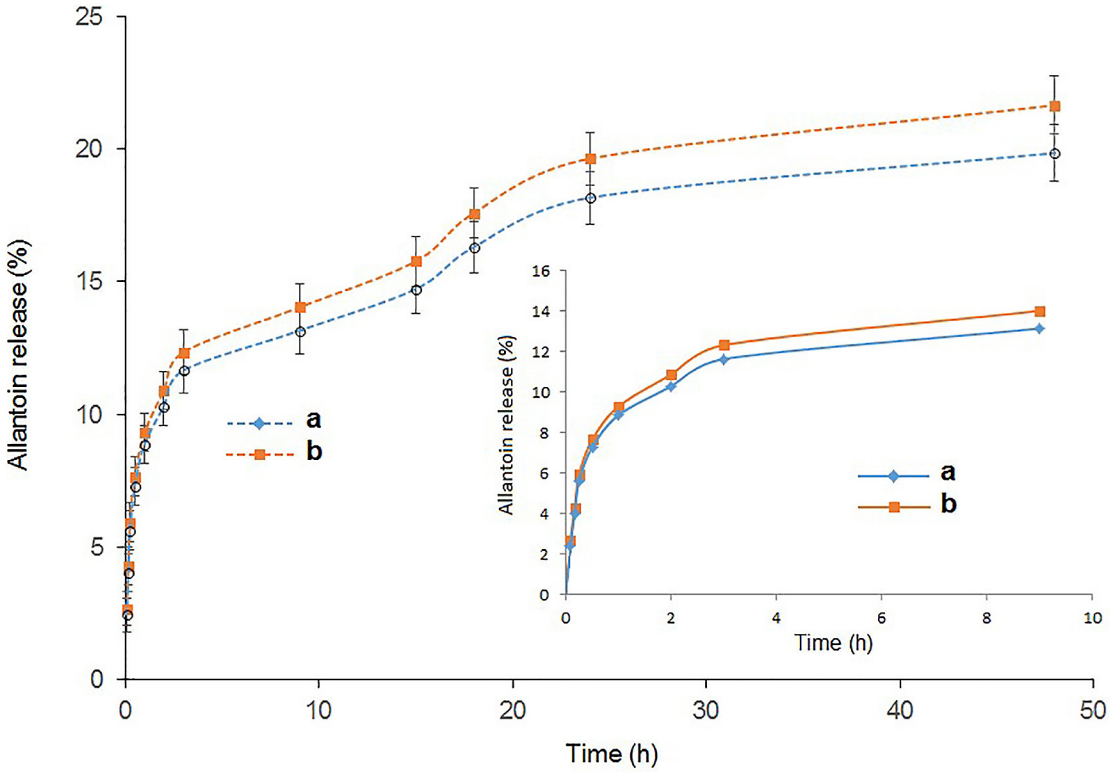

Figure 13. The allantoin release results of TMPE450-PU3-A:PCL (a) and TMPE1014-PU2-A:PCL (b).

Allantoin is suggested to play a significant role in promoting wound healing by influencing key cellular and molecular processes. Fibroblasts, essential for synthesizing collagen and other extracellular matrix components, are stimulated in their proliferation and migration by allantoin. This is crucial for tissue repair and the formation of granulation tissue, a vital step in wound healing. Furthermore, allantoin is believed to enhance collagen synthesis, providing structural support to tissues and contributing to effective wound healing. Its reported anti-inflammatory effects further create a favorable environment at the wound site. Therefore, the regular local release of allantoin in the wound field may accelerate the wound healing process, showcasing its potential as a beneficial agent in promoting tissue repair.

3.5. The Antibacterial Properties of Electrospun PU/PCL Wound Dressing Materials

The antibacterial properties of TMPE450-PU3-A:PCL and TMPE1014-PU2-A:PCL structures with different percentages of gentamicin doped were examined in Escherichia coli [(ATCC 25922), Gram (-)] and Bacillus subtilis [(ATCC 19659), Gram (+)] bacterial species. 1% of the gentamicin was added to the samples weighed as 0.1 g, and each sample was pelleted using 10 tons of pressure to obtain pellets with a diameter of approximately 1 cm. The resulting pellets were placed onto solid media containing bacteria, and the resulting petri dishes (Fig. 14) and zone diameters (mm) were given in Table 2.

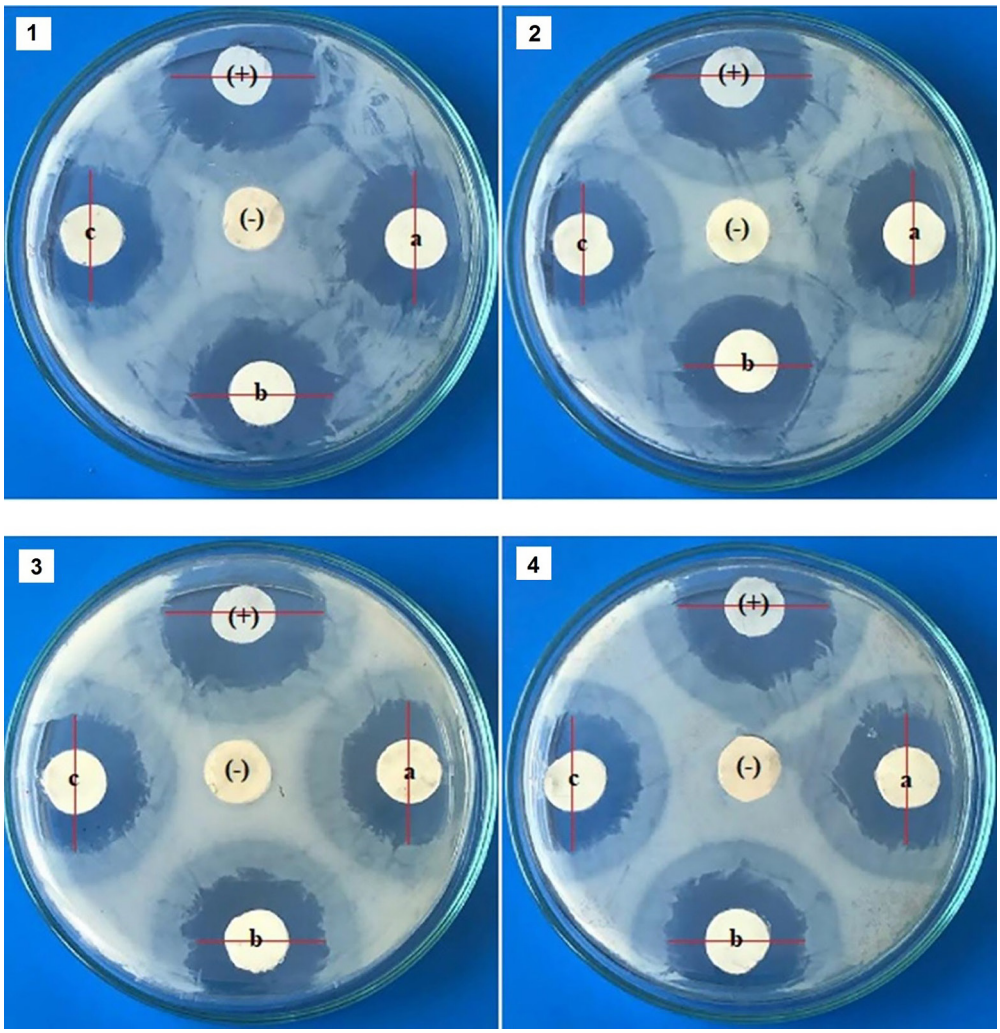

Figure 14. The zone diameters of gentamicin doped TMPE450-PU3-A:PCL-G polymer discs [(+) Control: TMPE450-PU3-A:PCL-G, a: TMPE450-PU3-A:PCL-G(%1), b: TMPE450-PU3-A:PCL-G(%3), c: TMPE450-PU3-A:PCL-G(%5), (-) Control: TMPE450-PU3-A:PCL-G] on Escherichia coli (Image 1), and the zone diameters of gentamicin doped TMPE450-PU3-A:PCL polymer discs [(+) Control: TMPE450-PU3-A:PCL-G, a: TMPE450-PU3-A:PCL-G(%1), b: TMPE450-PU3-A:PCL-G(%3), c: TMPE450-PU3-A:PCL-G(%5), (-) Control: TMPE450-PU3-A:PCL-G] on Bacillus subtilis (Image 2), and the zone diameters of gentamicin doped TMPE1014-PU2-A:PCL-G polymer discs [(+) Control: TMPE1014-PU2-A:PCL-G, a TMPE1014-PU2-A:PCL-G(%1), b: TMPE1014-PU2-A:PCL-G(%3), c: TMPE1014-PU2-A:PCL-G(%5), (-) Control: TMPE1014-PU2-A:PCL-G] on Escherichia coli (Image 3), and the zone diameters of gentamicin doped TMPE1014-PU2-A:PCL-G polymer discs [(+) Control: TMPE1014-PU2-A:PCL-G, a: TMPE1014-PU2-A:PCL-G(%1), b: TMPE1014-PU2-A:PCL-G(%3), c: TMPE1014-PU2-A:PCL-G(%5), (-) Control: TMPE1014-PU2-A:PCL-G] on Bacillus subtilis (Image 4).

When the results obtained for both bacterial species were examined, it was determined that all polymers containing 1% gentamicin showed antibacterial properties. In addition, it was observed that the polymer structures without gentamicin used as the (-) control group did not show any antibacterial effects. It was found that gentamicin used as (+) control was more effective than the synthesized polymers in terms of antibacterial effect.

In general, antibacterial activity assessments are crucial for wound dressings. Depending on the structure of antibacterial polyurethane used as wound dressing materials, most of the studies have two different kinds of bacteria in terms of Gram staining. For instance, in the study of Eskandarinia *et al.* in 2020, the antibacterial polyurethane-hyaluronic acid nanofibrous wound dressing was prepared. Then, an antibacterial activity assessment of this material was performed against E. coli and S. aureus via a zone of inhibition assay. They found that when the ratio of ethanolic extract of propolis increased in the polyurethane-hyaluronic acid wound dressings, the materials not only showed the highest antibacterial activities but also accelerated the in vivo wound healing process because of its biocompatibility as well (Eskandarinia *et al.*, 2020; Eskandarinia *et al.*, 2020).

Polymer	*E. coli* Zone Diameter (mm) Average ± Standard Deviation	*B. subtilis* Zone Diameter (mm) Average ± Standard Deviation
TMPE450-PU3-A:PCL-G-(+)	29.17 ± 1.33	32 ± 1.27
TMPE450-PU3-A:PCL-G-(%1)	27 ± 2.45	27.67 ± 2.34
TMPE450-PU3-A:PCL-G-(%3)	26 ± 1.79	26.17 ± 1.72
TMPE450-PU3-A:PCL-G-(%5)	26.33 ± 1.97	25.33 ± 1.63
TMPE450-PU3-A:PCL-G-(-)	—	—
TMPE1014-PU2-A:PCL-G-(+)	31.5 ± 0.84	33.17 ± 3.13
TMPE1014-PU2-A:PCL -G-(%1)	26.5 ± 1.87	27 ± 1.79
TMPE1014-PU2-A:PCL-G-(%3)	25.33 ± 1.63	27.83 ± 2.64
TMPE1014-PU2-A:PCL-G-(%5)	26 ± 1.1	26.67 ± 2.16
TMPE1014-PU2-A:PCL-G-(-)	—	—

Table 2. The zone diameters of gentamicin doped TMPE450-PU3-A:PCL and TMPE1014-PU2-A:PCL polymers

3.6. The Biocompatibility Properties of Electrospun PU/PCL Wound Dressing Materials

According to the biocompatibility test results, TMPE450-PU3-A:PCL and TMPE1014-PU2-A:PCL samples have 80.65±10.83%, 78.72±15.02% and 75.27±12.7% of cell viability rates and standard deviation values, respectively (Fig. 15). Depending on the biocompatibility values of the samples, it has been determined that TMPE450-PU3-A:PCL and TMPE1014-PU2-A:PCL have level 2 biocompatibility results. From Fig. 15, where the cell culture results in the biocompatibility test of the prepared samples can be seen, it can be concluded that TMPE450-PU3-A:PCL and TMPE1014-PU2-A:PCL samples do not have many morphological changes compared to the control group and therefore, their biocompatibility is high.

In the cell adhesion test, TMPE450-PU3-A:PLC (Fig 16(a)) and TMPE1014-PU2-A:PCL (Fig 16(b)) samples were incubated with L-929 mouse fibroblast cells for 1 week. TMPE450-PU3-A:PLC and TMPE1014-PU2-A:PCL samples were washed once with 70% ethanol and three times with PBS for five minutes. Then, each surface of the samples was sterilized under UV for 30 minutes. Later, one of the samples was placed in each well of the 24-well plate and L-929 mouse fibroblast cells were added to the samples with 500 µL of DMEM medium (containing 10% FBS and 1% Penicillin/Streptomycin) as $4x10^4$ cells/well. The media of the cells, which were incubated with the samples under the same conditions for 7 days, were replaced with fresh DMEM every two days. The samples were removed from the wells and washed with PBS to discard non-adherent cells from the samples at the end of the incubation period, and SEM analyses of these samples were performed (Fig. 16).

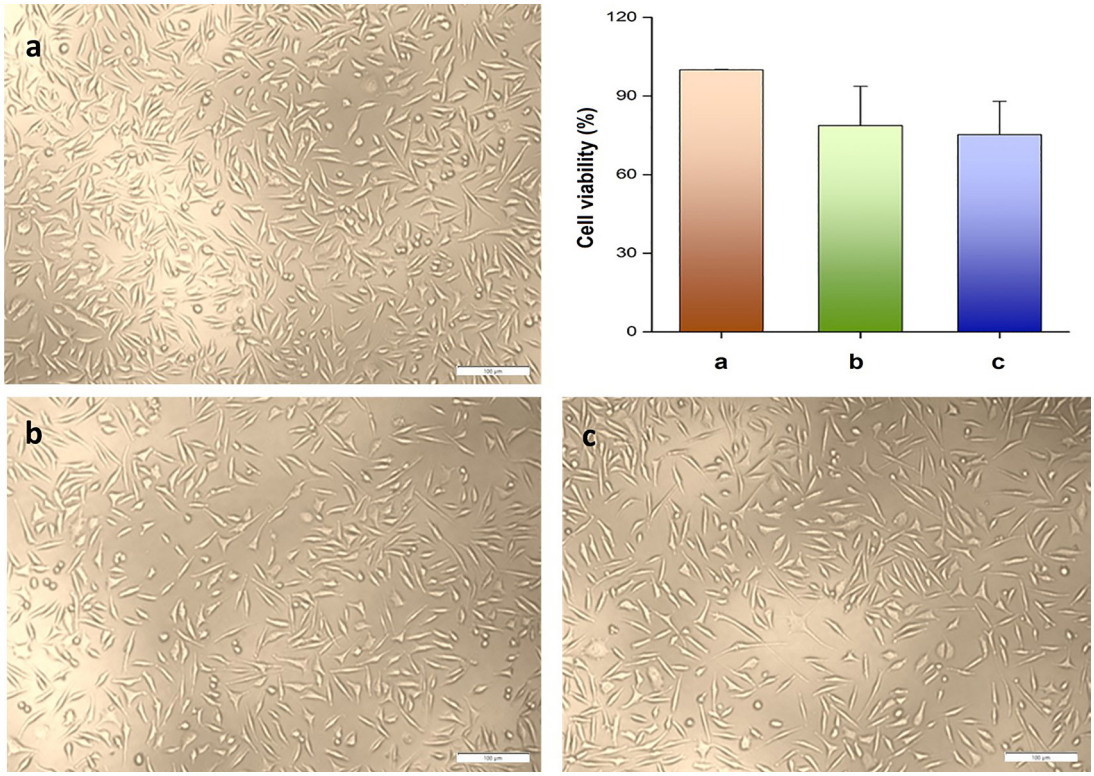

Figure 15. The biocompatibility test results of the prepared samples (a; control, b; TMPE450-PU3-A:PLC and c; TMPE1014-PU2-A:PCL; Magnifications of the images are 200X, white scale bars = 100 μm).

All of these results showed that these materials can allow cell proliferation and accelerate wound healing process. Besides, these presented data also demonstrated that our PU/PCL wound dressing material had similar cell viability values around 80% compared to the articles in the literature (Haryńska *et al.*, 2019). Furthermore, cell adhesion images proved that L-929 cells tended to attach onto our electrospun nanofibers manufactured from the synthesized PU/PCL polymer because of their low toxicity as well as easily promoting cell proliferation which is significant in wound healing progression.

4. CONCLUSION

In recent years, advancements in wound dressing materials have been notable. Nanotechnology applications, bioactive coatings, cellular therapies, and innovative materials with artificial intelligence support have emerged as key areas of progress. These developments aim to enhance wound healing efficacy, reduce infection risks, and improve patient comfort. Researchers focus on creating materials that are not only effective in promoting healing but also address specific challenges in wound care. In this study, aliphatic polyurethane structures were synthesized using TMPE molecules of different molecular masses. After their structural, thermal and mechanical properties were determined, polyurethane structures were transformed into wound dressing materials with PCL by electrospinning method. In addition, these materials also include gentamicin sulfate and allantoin to increase antibacterial and wound healing properties, respectively. The fiber structures and morphological properties of the TMPE based wound dressing materials were examined using SEM and AFM techniques. Fiber structures with smooth morphology, homogeneity and average diameter of 1300 and 1400 nm were determined. There are smooth spaces between the fiber structures that can allow the wound to breathe. The biocompatibility of the TMPE-based wound dressing materials was determined by *in vitro* cell culture tests. Approximately 80% cell viability was observed in these tests. In addition, allantoin and gentamicin were added to the structure of the resulting wound dressing materials to support their multi-functional effectiveness. Thanks to the

 https://doi.org/10.37819/nanofab.8.1787

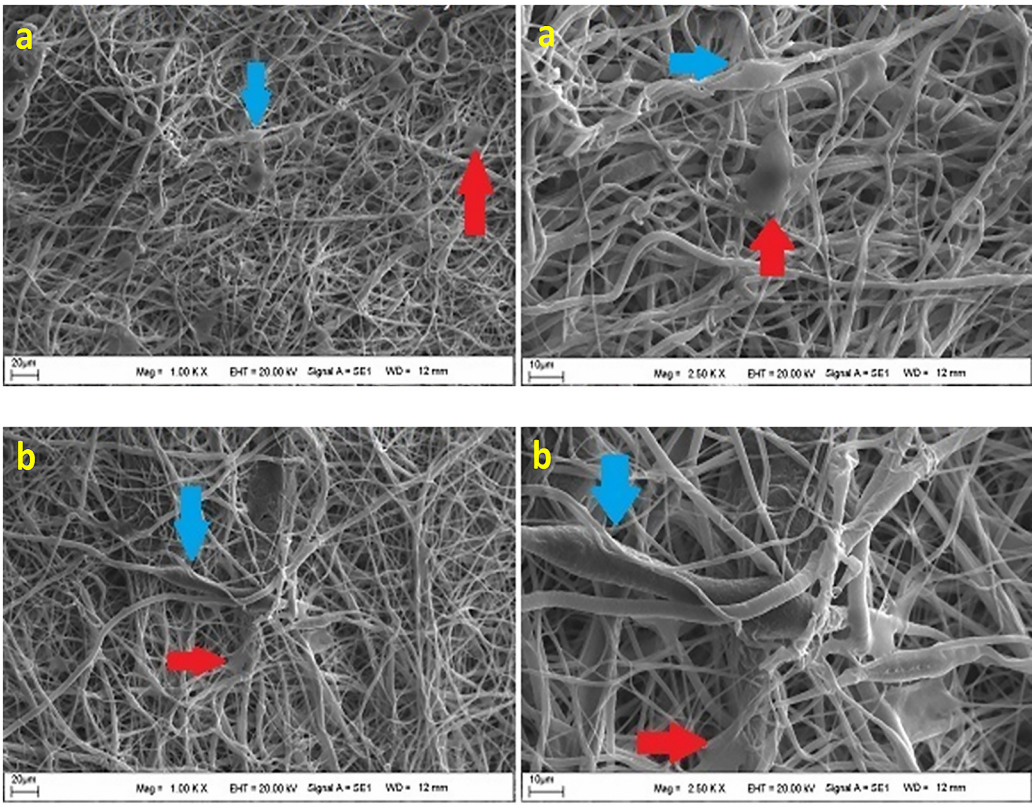

Figure 16. SEM images of L-929 cells adhered to TMPE450-PU3-A:PLC (a) and TMPE1014-PU2-A:PCL (b) samples at different magnifications (1000X and 2500X) (Red arrows indicate cells adhering to the samples, blue arrows show fiber beads formed during synthesis.)

antibacterial activity and regular delivery of allantoin, the wound-healing process will be increased by providing better wound care and accelerating the cell proliferation. As a result, the obtained wound dressing materials present an important alternative thanks to their high biocompatibility and multifunctional properties.

Acknowledgment

This work was financially supported by Inonu University Scientific Research Fund. ♦

REFERENCES

Bhoyar, S. D., Malhotra, K., & Madke, B. (2023). Dressing Materials: A Comprehensive Review. J. Cutan. Aesthet. Surg., 16(2), 81-89. https://doi.org/10.4103/JCAS.JCAS_163_22

Boateng, J. S., Matthews, K. H., Stevens, H. N. E., & Eccleston, G. M. (2008). Wound Healing Dressings and Drug Delivery Systems: A Review. Indian J. Pharml. Sci., 97, 2892-2923. https://doi.org/10.1002/jps.21210

Chaturvedi, A., Bajpai, A. K., Bajpai, J., & Singh, S. K. (2016). Evaluation of poly (vinyl alcohol) based cryogel-zinc oxide nanocomposites for possible applications as wound dressing materials. Mater. Sci. Eng., 65, 408-418. https://doi.org/10.1016/j.msec.2016.04.054

Chen, J. P., & Chiang, Y. (2010). Bioactive electrospun silver nanoparticles-containing polyurethane nanofibers as wound dressings. J. Nanosci. Nanotechnol., 10, 7560-7564. https://doi.org/10.1166/jnn.2010.2829

Chitrattha, S., & Phaechamud, T. (2016). Porous poly(dl-lactic acid) matrix film with antimicrobial activities for wound dressing application. Mater. Sci. Eng., 58, 1122-1130. https://doi.org/10.1016/j.msec.2015.09.083

Deitzel, J. M., Kleinmeyer, J. D., Hirvonen, J. K., & Beck Tan, N. C. (2001). Controlled deposition of electrospun poly(ethylene oxide) fibers.

Polymer, 42, 8163-8170. https://doi.org/10.1016/S0032-3861(01)00336-6

Demarre, L., Verhaeghe, S., Van Hecke, A., Clays, E., Grypdonck, M., & Beeckman, D. (2015). Factors predicting the development of pressure ulcers in an at-risk population who receive standardized preventive care: secondary analyses of a multicentre randomised controlled trial. J. Adv. Nurs., 71, 391-403. https://doi.org/10.1111/jan.12497

Dhivya, S., Padma, V. V., & Santhini, E. (2015). Wound dressings - a review. Biomedicine, 5(4), 22. https://doi.org/10.7603/s40681-015-0022-9

Eskandarinia, A., Kefayat, A., Agheb, M., Rafienia, M., Baghbadorani, M. A., Navid, S., Ebrahimpour, K., Khodabakhshi, D., & Ghahremani, F. (2020). A novel bilayer wound dressing composed of a dense polyurethane/propolis membrane and a biodegradable polycaprolactone/gelatin nanofbrous scafold. Scientific Reports, 10, 3063. https://doi.org/10.1038/s41598-020-59931-2

Eskandarinia, A., Kefayat, A., Gharakhloo, M., Agheb, M., Khodabakhshi, D., Khorshidi, M., Sheikhmoradi, V., Rafienia, M., & Salehi, H. (2020). A propolis enriched polyurethane-hyaluronic acid nanofibrous wound dressing with remarkable antibacterial and wound healing activities. International Journal of Biological Macromolecules, 149, 467-476. https://doi.org/10.1016/j.ijbiomac.2020.01.255

Haryńska, A., Kucinska-Lipka, J., Sulowska, A., Gubanska, I., Kostrzewa, M., & Janik, H. (2019). Medical-grade PCL based polyurethane system for FDM 3D printing—characterization and fabrication. Materials, 12, 887. https://doi:10.3390/ma12060887

Heyer, K., Augustin, M., Protz, K., Herberger, K., Spehr, C., & Rustenbach, S. J. (2013). Effectiveness of advanced versus conventional wound dressings on healing of chronic wounds: systematic review and meta-analysis. Dermatology, 226, 172-184. https://doi.org/10.1159/000348331

Kim, S., Park, S. G., Kang, S. W., & Lee, K. J. (2016). Nanofiber-based hydrocolloid from colloid electrospinning toward next generation wound dressing. Macromol. Mater. And Eng., 301, 818-826. https://doi.org/10.1002/mame.201600002

Kimel, K., Godlewska, S., Gleńsk, M., Gobis, K., Ośko, J., Grembecka, M., & Krauze-Baranowska, (2023). LC-MS/MS evaluation of pyrrolizidine alkaloids profile in relation to safety of comfrey roots and leaves from Polish sources. Molecules, 28, 6171. https://doi.org/10.3390/molecules28166171

Lee, S. J., Heo, D. N., Moon, J. H., Park, H. N., Ko, W. K., Bae, M. S., Lee, J. B., Park, S. W., Kim, E.c., Lee, C. H., Jung, B. Y., & Kwon, I. K. (2014). Chitosan/polyurethane blended fiber sheets containing silver sulfadiazine for use as an antimicrobial wound dressing. J. Nanosci. Nannotechnol., 14, 7488-7494. https://doi.org/10.1166/jnn.2014.9581

Lionelli, G. T., & Lawrence, W. T. (2003). Wound dressings. Surg. Clin. North Am., 83, 617-638.

Liu, M., Duan, X. P., Li, Y. M., Yang, D. P., & Long, Y. Z. (2017). Electrospun nanofibers for wound healing. *Materials Sci. and Eng. C.*, *76*, 1413-1423. https://doi.org/10.1016/j.msec.2017.03.034.

Mehteroğlu, E., Çakmen, A., Aksoy, B., Balcioğlu, S., Köytepe, S., Ateş, B., & Yilmaz, İ. (2020). Preparation of hybrid PU/PCL fibers from steviol glycosides via electrospinning as a potential wound dressing materials. Journal of Applied Polymer Science, 49217. https://doi.org/10.1002/app.49217

Miguel, S. P., Ribeiro, M. P., Brancal, H., Coutinho, P., & Correia, I. J. (2014). Thermoresponsive chitosan-agarose hydrogel for skin regeneration. Carbohydr. Polym., 111, 366-373. https://doi.org/10.1016/j.carbpol.2014.04.093

Mogoşanu, G. D., & Grumezescu, A. M. (2014). Natural and synthetic polymers for wounds and burns dressing. Int. J. Pharm., 463, 127-136. https://doi.org/10.1016/j.ijpharm.2013.12.015

Nastić, N., Borrás-Linares, I., Lozano-Sánchez, J., Švarc-Gajić, J., & Segura-Carretero. (2020). Comparative assessment of phytochemical profiles of comfrey (Symphytum officinale L.) root extracts obtained by different extraction techniques. Molecules, 25(4), 837. https://doi.org/10.3390/molecules2504083

Nguyen, H. M., Le, T. T. N., Nguyen, A. T., Le, H. N. T., & Pham, T. T. (2023). Biomedical materials for wound dressing: recent advances and applications. RSC Adv., 13, 5509-5528. https://doi.org/10.1039/D2RA07673J

Pierchala, M. K., Makaremi, M., Tan, H. L., Pushpamalar, J., Muniyandy, S., Solouk, A., Lee, S. M., & Pasbakhsh, (2018). Nanotubes in nanofibers: Antibacterial multilayered polylactic acid/halloysite/gentamicin membranes for bone regeneration application. App. Clay Sci., 160, 95-105. https://doi.org/10.1016/j.clay.2017.12.016

Pyun, D. G., Choi, H. J., Yoon, H. S., Thambi, T., & Lee, D. S. (2015). Polyurethane foam containing rhEGF as a dressing material for healing diabetic wounds: synthesis, characterization, *in vitro* and in vivo studies. Colloids Surf., 135, 699-706. https://doi.org/10.1016/j.colsurfb.2015.08.029

Sahraro, M., Yeganeh, H., & Sorayya, M. (2016). Guanidine hydrochloride embedded polyurethanes as antimicrobial and absorptive wound dressing membranes with promising cytocompatibility. Mater. Sci. Eng., 59, 1025-1037. https://doi.org/10.1016/j.msec.2015.11.038

Singh, B., Sharma, S., & Dhiman, A. (2013). Design of antibiotic containing hydrogel wound dressings: Biomedical properties and histological study of wound healing. Int J. Pharm., 457, 82-91. https://doi.org/10.1016/j.ijpharm.2013.09.028

Staiger, C (2013). Comfrey root: From tradition to modern clinical trials. Wien. Med. Wochenschr., 163, 58-64. https://doi.org/10.1007/s10354-012-0162-4

Xu, R., Luo, G., Xia, H., He, W., Zhao, J., Liu, B., Tan, J., Zhou, J., Liu, D., Wang, Y., Yao, Z., Zhan, R., Yang, S., & Wu, J. (2015). Novel bilayer wound dressing composed of silicone rubber with particular micropores enhanced wound re-epithelialization and contraction. Biomaterials, 40, 1-11. https://doi.org/10.1016/j.biomaterials.2014.10.077

Xu, R., Xia, H., He, W., Li, Z., Zhao, B., Liu, B., Wang, Y., Lei, Q., Kong, Y., Bai, Y., Yao, Z., Yan, R., Li, H., Zhan, R., Yang, S., Luo, G., & Wu, J. (2016). Controlled water vapor transmission rate promotes wound-healing via wound re-epithelialization and contraction enhancement. Sci. Rep., 6, 24596. https://doi.org/10.1038/srep24596

Xu, W. T., Ma, C. F., Ma, J. L., Gan, T. S., & Zhang, G. Z. (2014). Marine biofouling resistance of polyurethane with biodegradation and hydrolyzation. ACS Appl. Mater. Interfaces., 6, 4017-4024. https://doi.org/10.1021/am4054578

Yao, C. H., Lee, C. Y., Huang, C. H., Chen, Y. S., & Chen, K. Y. (2017). Novel bilayer wound dressing based on electrospun gelatin/keratin nanofibrous mats for skin wound repair. Mater. Sci. Eng. C Mater. Biol. Appl., 79, 533-540. https://doi.org/10.1016/j.msec.2017.05.076

Yan, L., Si, S., Chen, Y, Yuan T., Fan H., Yao Y., Zhank Q. (2011) Electrospun in-situ hybrid polyurethane/nano-TiO_2 as wound dressings. Fibers Polym. 12, 207-213. https://doi.org/10.1007/s12221-011-0207-0.

Yudanova, T. N., & Reshetov, I. V. (2006). Modern wound dressings: Manufacturing and properties. Pharm. Chem. J., 40, 85-92.

Zahedi, P., Rezaeian, I., Ranaei-Siadat, S. O., Jafari, S. H., & Supaphol, P. (2009). A review on wound dressings with an emphasis on electrospun nanofibrous polymeric bandages. Polym. Adv. Technol., 21, 77-95. https://doi.org/10.1002/pat.1625